



HAL
open science

Modelling of the conductive heat transfer through nano-structured porous silica materials

R Coquard, D. Baillis, V Grigorova, Franck Enguehard, D Quenard, P Levitz

► **To cite this version:**

R Coquard, D. Baillis, V Grigorova, Franck Enguehard, D Quenard, et al.. Modelling of the conductive heat transfer through nano-structured porous silica materials. *Journal of Non-Crystalline Solids*, 2013, 363, pp.103-115. 10.1016/j.jnoncrysol.2012.11.053 . hal-01287425

HAL Id: hal-01287425

<https://hal.science/hal-01287425>

Submitted on 7 Jun 2023

HAL is a multi-disciplinary open access archive for the deposit and dissemination of scientific research documents, whether they are published or not. The documents may come from teaching and research institutions in France or abroad, or from public or private research centers.

L'archive ouverte pluridisciplinaire **HAL**, est destinée au dépôt et à la diffusion de documents scientifiques de niveau recherche, publiés ou non, émanant des établissements d'enseignement et de recherche français ou étrangers, des laboratoires publics ou privés.

Modeling of the Conductive Heat Transfer through Nano-structured Silica Materials

R. Coquard¹, D. Baillis², V. Grigorova-Moutiers³, F. Enguehard⁴, D. Quenard⁵ and P. Levitz⁶

Abstract

There is currently a growing interest in nano-structured silica based materials due to their remarkable thermal properties. These materials are notably used in Vacuum Insulating Panels (VIP). Their exceptional insulating performances have been demonstrated experimentally for a relatively long time. But the heat transfer mechanisms occurring in this kind of materials remain relatively badly known due to the nanometric dimensions and to the complexity of the porous structure. Therefore, the present study aims to develop a numerical model for estimating the magnitude of conductive heat transfer inside nano-structured silicas using a theoretical representation of their complex porous structure. The model takes into account the special porous morphology of the materials at both the nanometric and microscopic scale. Moreover, the conduction heat transfer at the nanometric scale is treated using a numerical resolution of the Boltzmann Equation since the validity of the macroscopic laws is then questionable. The computations are conducted using phonon properties of silica obtained in the literature. A parametric study allows us to analyse the influence of structural characteristics and thermo-physical properties on the insulating performances and thus to highlight the most important parameters.

¹ Société (EC2-MODELISATION) ; 66, boulevard Niels Bohr, 69603 Villeurbanne CEDEX, France. **Phone:** +33 (0)4 37 48 84 37; **FAX:** 04 37 48 84 05 **Email:** remi.coquard@ec2-modelisation.fr

² Laboratoire de Mécanique des Contacts et des Solides (LAMCOS), UMR CNRS / INSA Lyon 5514, 20 rue des Sciences, 69621 Villeurbanne Cedex, France. **Phone:** 04 72 43 84 74 **Email :** dominique.baillis@insa-lyon.fr

³ SAINT-GOBAIN RECHERCHE Service TMM, 39, quai Lucien Lefranc, B. P. 135 93303 Aubervilliers Cedex, **Phone:** +33 (0)1 48 39 59 54 **Email :** veneta.grigorova-moutiers@saint-gobain.com

⁴ CEA/Le Ripault, BP 16, 37260 Monts, France. **E-mail:** franck.enguehard@cea.fr

⁵ Centre Scientifique et Technique du Bâtiment (CSTB), 24 rue Joseph FOURIER, 38400 Saint Martin d'Hères, France. **Phone :** +33 (0)4 76 76 25 46 **Email :** daniel.quenard@cstb.fr

⁶ Laboratoire de Physique de la Matière Condensée (LPMC), CNRS UMR 7643, Ecole Polytechnique, 91128 Palaiseau Cedex, **Email :** pierre.levitz@polytechnique.edu

Nomenclature

A (m²): area of (x,y) plans of the box simulating the guarded hot-plate for two-particles in contact

$C_s(\omega, T)$ (J/m³/K): Specific Heat

$D_p(\omega, T)$ (m⁻³): Phonon density of states per unit volume

D_c (m): Contact Diameter between two neighbouring nano-particles

D_p (m): particle diameter

f_v : solid fraction

h (m): width of the box simulating the guarded hot-plate apparatus for the arrangement of aggregates

$k_{p \rightarrow p}$ (W/m/K): particle-particle thermal conductivity between two neighbouring particles

k_{eff} (W/m/K): effective thermal conductivity of the nano-structured silica based material

$k_f, k_{f, \text{free}}$ (W/m/K): thermal conductivity of the confined and free fluid

k_0 : prefactor

k_B : Stefan-Boltzmann constant $k_B = 5.67 \times 10^{-8} \text{ kg} \cdot \text{s}^{-3} \text{K}^{-4}$

\vec{K} (W/m/K): thermal conductivity tensor

L_g (m): mean free path of gas molecules at atmospheric pressure

$n(\mathbf{t}, \vec{s})$: Phonon distribution function

P (Pa): gas pressure

\vec{q} (W/m²): heat flux due to phonon transport

s (m): curvilinear abscissa

t (s): time

T (K): temperature

T_h (K): hot plate temperature

T_c (K): cold plate temperature

t_p (m): pore characteristic size

v_s (m/s): phonon group velocity

x, y, z : Cartesian coordinates

Greek symbols

Λ (m): Phonon mean free path

ω (s⁻¹): Phonon frequency

ω_D (s⁻¹): Debye frequency

ε : porosity

σ_0 (m²): gas molecules cross-section

Φ_c (W): conductive heat flux

1 Introduction

Among different business, building domain is the most energy consuming one with more than 45% of the total energy, far more than the industry (28%) or transport fields. Most of this energy is devoted to the building heating. Therefore, the thermal insulation quality is of primary importance; the improvement of thermal insulators performances of is a major issue in view of a significant reduction in the global energy consumption. Current researches are interested in the development of new insulating materials, notably nanoporous silica-based superinsulating materials. These materials are made of silica particles, forming aggregates in several nanometres of diameter, which are themselves agglomerated in highly porous matrix ($\epsilon \approx 90\%$). This nanostructured silica presents a double-scale structure: (i) at the nanometric scale aggregates form chains of silica particles with undividable links; and (ii) at the microscopic scale, the structure is formed by aggregates agglomeration. Nano-structured silica structure is illustrated in Figure 1, visualizing fumed silica formation process of when chlorosilanes molecules are introduced inside a flame.

The good insulating properties of nanostructured silicas are due to the very small pores size of the: pores are from the same order of magnitude as the mean free path of air molecules. Indeed, according to Kaganer [1], the thermal conductivity of a confined gas can be expressed by:

$$k_f = \frac{k_{f.free}}{1 + \frac{\sqrt{2} \cdot \beta \cdot k_B \cdot T}{\sigma_0 \cdot (t_p \cdot P)}} = \frac{k_{f.free}}{1 + 2 \cdot \beta \cdot \frac{L_g}{t_p}} \quad (1)$$

where the mean free path of the gas molecules L_g and the constant β can be calculated by

$$L_g = \frac{k_B T}{\sqrt{2} \cdot \sigma_0 \cdot P} \quad \text{and} \quad \beta = \frac{5\pi}{32} \cdot \frac{2 - \alpha}{\alpha} \cdot \frac{9\gamma - 5}{\gamma + 1} \quad \text{with } \alpha \text{ the accommodation coefficient and } \gamma \text{ the}$$

adiabatic coefficient. For air, the adiabatic coefficient γ was set to 1.4 and for the accommodation coefficient $\alpha = 1$ was applied.

Thus, under partial vacuum, air thermal conductivity, which is the main part of the superinsulants total thermal conductivity, gets reduced because of the “Knudsen effect (non-confined air conductivity is $k_{\text{air}} \approx 25 \text{ mW/m/K}$ while for good commercial insulators total conductivity is typically comprised between 30 and 40 mW/m/K). In such a case, heat transfer mainly occurs by thermal conduction through the solid phase and by thermal radiation propagation. Besides, the nanostructured silicas currently commercialised generally contain additional opacifying micrometric particles in order to reduce drastically the contribution of radiation heat transfer. Then, when a primary vacuum is applied and when opacifying particles are added, equivalent thermal conductivities lower than 10mW/m/K can be achieved as reported by Quenard et Sallée [2] or the researchers of ZAE Bayern [3-6]. This constitutes a substantial improvement of insulating properties compared to the most performing classical insulators.

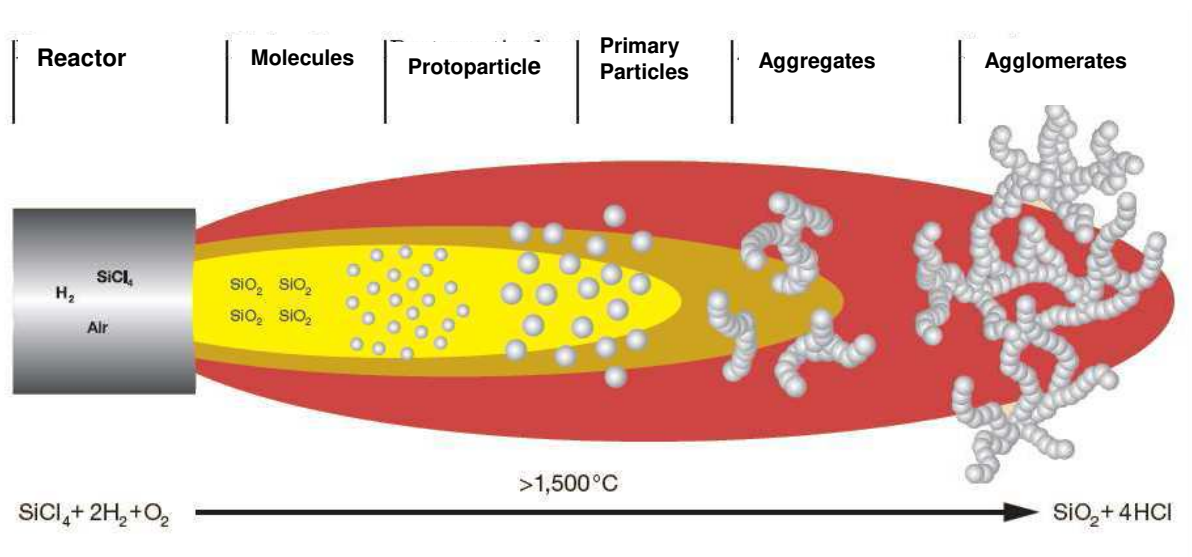


Figure 1: Illustration of fumed silica formation process: Different stages of aggregation and agglomeration

Because of the growing interest for these materials, numerous recent studies have been devoted to experimental or theoretical characterization of the heat transfer in nano-structured silicas.

Their outstanding thermal properties have been demonstrated experimentally for a relatively long time. For example, Quenard et Sallée [2] have analysed samples with porosities higher than 90% composed of fumed silicas combined with micrometric fibres insuring the mechanical strength and opacifying particles. At ambient pressure and temperature, the equivalent conductivity was about 20mW/m/K and can be reduced to 6mW/m/K when a primary vacuum such as 1-10 hPa is applied. The noticeable increase of this conductivity with temperature reported by the authors suggests that a significant part of the heat transfer is due to thermal radiation. Similarly, the researchers of ZAE Bayern [3-6] have measured equivalent thermal conductivities close to 3mW/m/K for evacuated and opacified porous materials based on nano-structured silicas at ambient temperature.

In parallel, several theoretical studies have been initiated in order to model the thermal transfer in silica-based super-insulating materials. Coquard and Quenard [7] have proposed a model of computation of their equivalent conductivity taking into account the radiation-conduction coupling. The effective thermal conductivity (conductive transfer alone) was estimated using a Finite Volume Model considering the heat conduction through gas and solid phase. The authors assumed that the macroscopic laws of heat conduction are valid at the nanoscale. They depicted the structure of nano-structured silicas as chains of silica grains distributed at the edges of a cubic network. They studied the influence of air pressure and of the contact area between two particles touching each other. The results of their model highlighted the influence of the air pressure. The effective conductivities computed were in good agreement with the values measured at the CSTB [2] or ZAE Bayern [3-6] for different air pressures. The numerical results also highlighted the influence of the particle diameter and

the contact area between neighbouring particles. Rochais, Domingues and Enguehard [8] have also developed a model of computation of the effective conductivity of silica-based nanoporous super-insulating materials. They applied Finite Volume computations to different 2-D or 3-D fractal structures to evaluate the influence of the solid fraction on the conductivity. Finally, during its ph-D, Spagnol [9] have used a Finite Difference Method to solve numerically the heat conduction equation through various fractal geometries. Like in preceding studies [7, 8], the author considered the macroscopic heat conduction laws to be valid and used Eq. (1) for estimating the gas conductivity. Computations were applied to simple fractal geometries like brick walls, Von Koch flakes and to random fractal geometries obtained by diffusion limited aggregation process.

These first theoretical studies permitted to highlight the main mechanisms responsible for conductive heat transfer in nano-structured silica-based materials and to point out the parameters that mostly affect the effective conductivity. However, all these studies considered the macroscopic Fourier law of heat conduction ($\phi_c = -\vec{K} \cdot \text{grad}T$) as valid at nanoscale. However, according to Kittel [10], the phonon mean free path in silica is about one to several nm and is therefore non-negligible compared to the particle size. Thus, the validity of the macroscopic laws is questionable. In view of the models improvement, it seems indispensable to use another approach for treating conduction heat transfer at the nanometric scale.

Besides, recent studies are initiated to account for the “nanoscopic effects”, using notably Molecular Dynamics (MD) simulations. However, the works which are interested specifically in the heat transfer between two silica nano-particules remain relatively rare and have been conducted essentially by Domingues et al. [11, 12] and Mahajan et al. [13]. Domingues et al. have estimated the thermal conductance between two particles in contact [12] or separated by a submicronic distance [11]. For this purpose, they used the fluctuation-dissipation theorem and applied a MD computation. For silica particles in contact with

diameters comprised between 1.5 and 5 nm, they showed that the thermal conductance is proportional to the number of atoms in contact. Then, they managed to compute an “atomic” conductance which is comprised between 0.5 and 3 nW/K. This leads to a total heat exchange between two particles of about 1 to 2 μW per nm^2 of contact area. Similarly, Mahajan, Subbarayan and Sammakia [13] have estimated the thermal conductivity of silica nanoparticles by MD simulations using the Green-Kubo relations. They applied their computations to silica particle composed of 600 atoms (several nm in diameter) and obtained a thermal conductivity of 0.59 W/m/K corresponding to approximately 40-50% of the silica at the macroscopic scale. These results show the significant influence of the particle size at the nanometric scale. MD simulations are promising and give rise to a growing interest. However, the two preceding studies have highlighted their major drawback: they require high computation costs and time when dimensions of several nm or tenth of nm are considered. This is prohibitive in view of parametric studies. Moreover, they require highly specific and sharp scientific skills.

Other numerical methods have been developed to model the heat transfer at nanometric scale when macroscopic laws are invalid. The most common one consists in solving the Boltzmann equation governing the phonon transport inside nano-structured materials. This approach can be used for dielectric or semiconductor materials for which phonons are the unique heat carriers (the contribution of electron is negligible). This method is rigorously applicable only when the smallest dimension is more important than the phonon wavelength so that the phonons can be considered as massless particles by neglecting the interference between phonon waves. It has been largely used for estimating the thermal conductivity of silicon-based nanostructures notably by Mazumder and Majumdar [14] Lacroix et al. [15, 16] or Randrianalisoa et Baillis [17-20]. These authors resorted to Monte Carlo procedure for the resolution of the Boltzmann Equation. The principle of this approach

is to follow the path of a great number of phonons emitted by the materials and carrying thermal energy. Each phonon has its own wavelength and polarisation. During their path, the phonons can undergo phonon-phonon scattering, scattering by impurities or defaults, can be reflected at the interface between the phases or be absorbed at the boundary surfaces of the system or inside the material. The phonon properties required are: (1) the phonon mean free path before interaction with other phonons or with impurities/defaults; (2) the phase velocities; (3) the group velocities; (4) the density of states; (5) the heat capacity; and (6) dispersion curves. Each of these properties varies with the frequency and the polarisation of the phonon. Due to the numerous applications of silicon in microelectronics where the size of the components might be submicronic, its phonon properties have been extensively characterized. Mazumder and Majumdar [14], Lacroix et al. [15, 16] and Randrianalisoa and Baillis [17, 18] have computed the thermal conductivity of very thin silicon films and have shown that it gets lower than the macroscopic conductivity when the thickness of the film is from the same order of magnitude as the phonon mean free paths. Lacroix [16] and Randrianalisoa and Baillis [18] have also investigated the conductivity of silicon nano-wires while Randrianalisoa and Baillis [20] have applied the method to nanoporous silicon films of various thicknesses. They managed to estimate the influence of the porous characteristics (porosity, pore size, shape of pores) on their conductivity.

The Boltzmann equation numerical resolution via Monte Carlo procedures is very interesting for the present study problem as it permits to take into account accurately the morphology of the porous structure as well as it is well-adapted to the dimensions of the nano-structured silica materials particles. That is the reason why, this approach is used in the present study for evaluating the heat exchange between two neighbouring particles. For simplicity purpose, the particles are assumed spherical with homogeneous diameter.

Once the heat exchange between nano-particles has been evaluated, the proposed model should also take into account the morphology of the nano-structured silica at the microscopic scale. This has been done by assimilating the material to a random agglomeration of aggregates composed of silica particles chains. According to previous studies [21-23], these aggregates present a fractal like structure. Thereafter, the effective conductivity of this agglomeration of aggregates is evaluated by simulating a 1-D heat transfer across a slab of material. The heat transfer problem is solved using a Finite Volume Scheme. The obtained numerical results allow us to study the evolution of the silica-based nano-structured materials effective conductivity with air pressure, structural parameters (such as diameter of particles, contact area between particles, fractal characteristics, size of aggregates) and material thermo-physical properties.

2 Heat Transfer Model

2.1 Representation of the nano-porous structure

As explained in the introduction, the nano-structured silicas consist of randomly organized agglomerates of aggregates (see Figure 2). The aggregates are made of chains of silica particles related among them by undividable connections. The silica particles are assumed spherical with a unique diameter denoted by D_p . The contact area between two neighboring particles is characterized by a contact diameter denoted D_c .

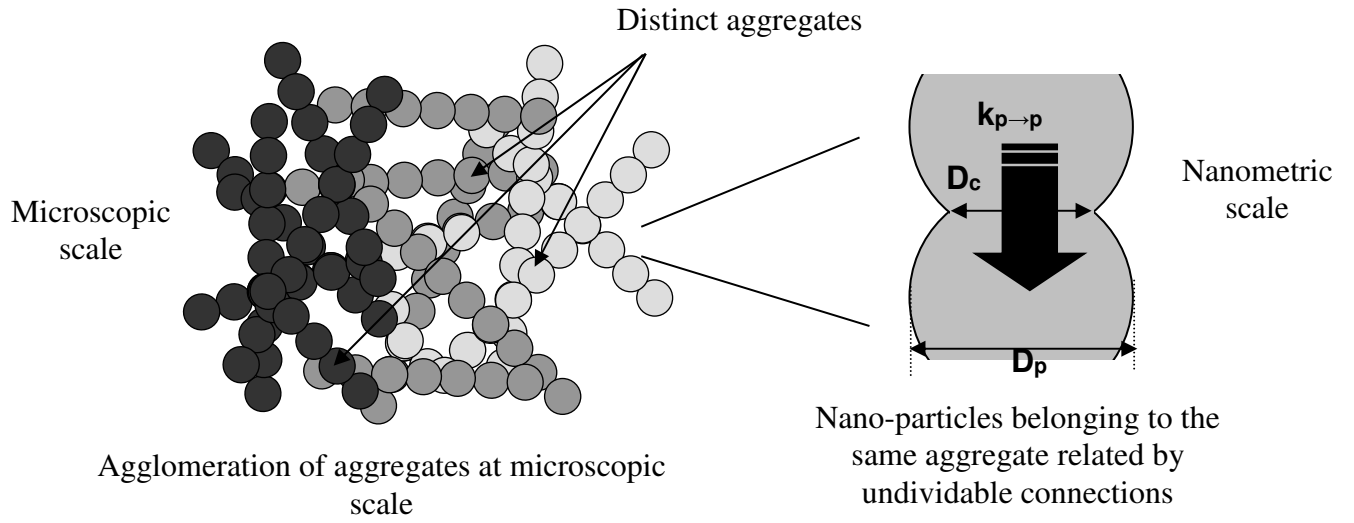


Figure 2 : Illustration of nano-structured silicas organization at microscopic and nanometric scales

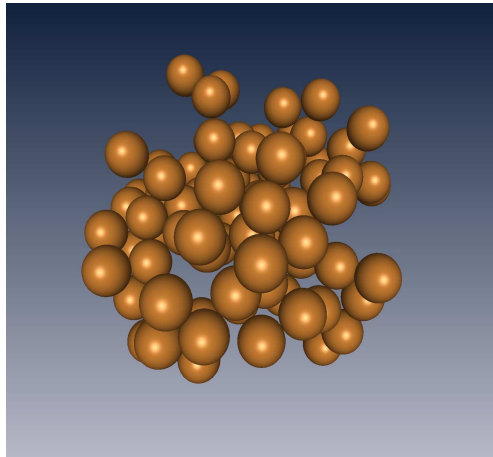
Each aggregate, composed of N_p particles, is assumed to have a fractal like structure, i.e. the number of particles comprised in a sphere with radius R_g centred on the aggregate can be expressed by:

$$N(R_g) = k_0 \left(\frac{R_g}{D_p / 2} \right)^{D_f} \quad (2)$$

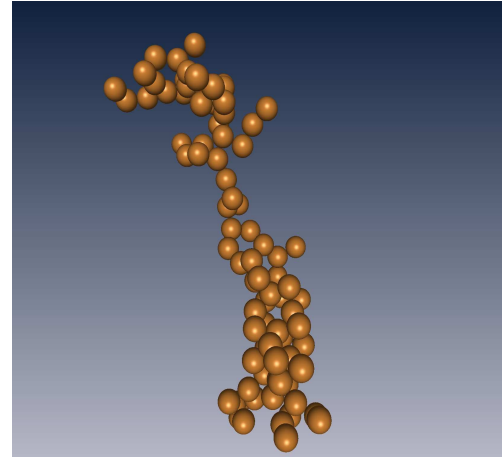
where D_f is the fractal dimension and k_0 the prefactor.

The aggregates are generated using the Sequential Algorithm (SA) described by Mackovski [24]. The agglomeration is conducted using a particle-cluster procedure and the principle is to add particles one by one successively by checking at each stage that Eq. (2) is fulfilled. The variations of the aggregates morphology with the D_f and k_0 values are illustrated on Fig. 3: we depict aggregates of 88 particles with three different combinations of D_f and k_0 , namely $(D_f=1.8, k_0=1.1)$; $(D_f=2.5, k_0=1.1)$; $(D_f=1.8, k_0=1.5)$. Aiming to visualize the large range of compacity that can be obtained by varying D_f and k_0 only, the three representations have different length scales.

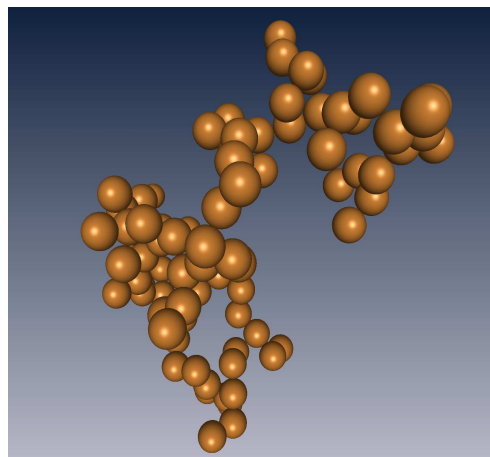
It can be noted that the fractal dimension seems to have an important influence on the aggregates compacity since the aggregates with high values of D_f are noticeably more compact.



$D_f = 2.5; k_0 = 1.1$



$D_f = 1.8; k_0 = 1.1$



$D_f = 1.8; k_0 = 1.5$

Figure 3: Illustration of 3 representative aggregates with the same number of particles but different values of fractal dimension and prefactor

2.2 Modeling of the heat exchange between two nano-particles in contact

The Boltzmann equation resolution via Monte Carlo procedure has already demonstrated its relevance for the modelling of the conduction heat transfer at the nanometric scale, notably through silicon nanometric structures [14-20]. We have adapted the method for

treating heat exchange between two neighbouring nano-particles belonging to the same aggregates. This heat exchange is characterised by the so-called “particle-particle” conductivity denoted $k_{p \rightarrow p}$; it quantifies the conductive thermal transport intensity between the spherical particles centres. This conductivity will then be used for estimation of heat exchange through the entire agglomerated structure.

2.2.1 Phonon properties of silica

Solving the Boltzmann equation in silica nano-structures requires the silica phonon properties. Phonon transport in silica, however, has been noticeably less studied than in silicon and that data remain relatively rare. Kittel [10] was the first to analyse the conductivity measurement of glass in order to propose a mean free path for phonons in silica. Stephens [25], Freeman and Anderson [26] and Love et Anderson [27] have also studied experimentally the variations of the thermal conductivity of glasses with temperature and proposed some models expressing the phonon mean free paths at different frequencies. More recently, Goodson et al. [28] have collected the experimental data proposed by several researchers concerning the phonon properties (Kittel [29], Stephens [25], Hunklinger and Arnold [30], Gilroy et Philips [31], Bonnet [32], Zaitlin et al. [33]) in order to develop a model for computation of thin silica films thermal conductivity. They showed that, due to the scattering of phonons by the boundaries, silica films conductivity at low temperatures decreases with the thickness when the thickness is lower than few μm . The specific heat and conductivity of the films were calculated using the Debye model whereas the phonon mean free paths were obtained by separating the frequency spectrum in three different zones. To our knowledge, the model used by Goodson et al. [28] is the most comprehensive one and we decided to use it for the resolution of the Boltzmann equation in silica at the nanometric scale. The phonon properties given by the model are:

- Debye Angular Frequency $\omega_D = 6.441 \times 10^{13} \text{ rad.s}^{-1}$

- Average speed of sound $v_s = 4100 \text{ m.s}^{-1}$
- Specific Heat $C_s(x_\omega, T) = 9.N_a.k_B.\left(\frac{T}{\theta}\right)^3 \cdot \frac{x_\omega^4 \cdot \exp(x_\omega)}{(\exp(x_\omega) - 1)^2}$ with $x_\omega = \frac{h_P \cdot \omega}{k_B \cdot T}$;
 $N_a = 6.62 \times 10^{28} \text{ m}^{-3}$; $\theta = 492 \text{ K}$; $k_B = 1.38 \times 10^{-23} \text{ J/K}$, the Boltzmann constant, $h_P = 1.054 \times 10^{-34} \text{ J.s}$ the Planck constant
- Phonon density of states $D_p(x_\omega, T) = \frac{C_s(x_\omega, T) \times (\exp(x_\omega) - 1)^2}{x_\omega^2 k_B \exp(x_\omega)} = 9.N_a \left(\frac{T}{\theta}\right)^3 x_\omega^2$
- Phonon mean free paths: $\Lambda = 0.45 \text{ nm}$ for $\omega > 0.1 \times \omega_D$; $\Lambda(\omega) = \frac{S_D}{\omega^4}$ for $0.1 \times \omega_D > \omega > 0.01 \times \omega_D$; $\frac{1}{\Lambda(\omega, T)} = \frac{\pi.S_{SR}.\omega}{2.v_s} \left[\frac{\Gamma\left(\frac{T^*}{2} + 1\right)}{\sqrt{\pi} \cdot \Gamma\left(\frac{T^*}{2} + \frac{3}{2}\right)} \cdot \frac{T^*}{\cos\left(\frac{\pi}{2} T^*\right)} (\omega^*)^{T^*} - \frac{T^*}{1 - T^*} \cdot \omega^* \right]$ for $0.01 \times \omega_D > \omega$. With
 $\omega^* = \omega \cdot \tau_0$; $T^* = k_B.T/E_0$; $S_D = 1.76 \times 10^{42} \text{ m.rad}^4.\text{s}^{-4}$; $E_0 = 5.02 \times 10^{-21} \text{ J}$; $\tau_0 = 2.5 \times 10^{-13}$
and $S_{SR} = 1.89 \times 10^{-3}$.

The variations of the phonon mean free paths with frequency at different temperatures are illustrated on Fig. 4. .

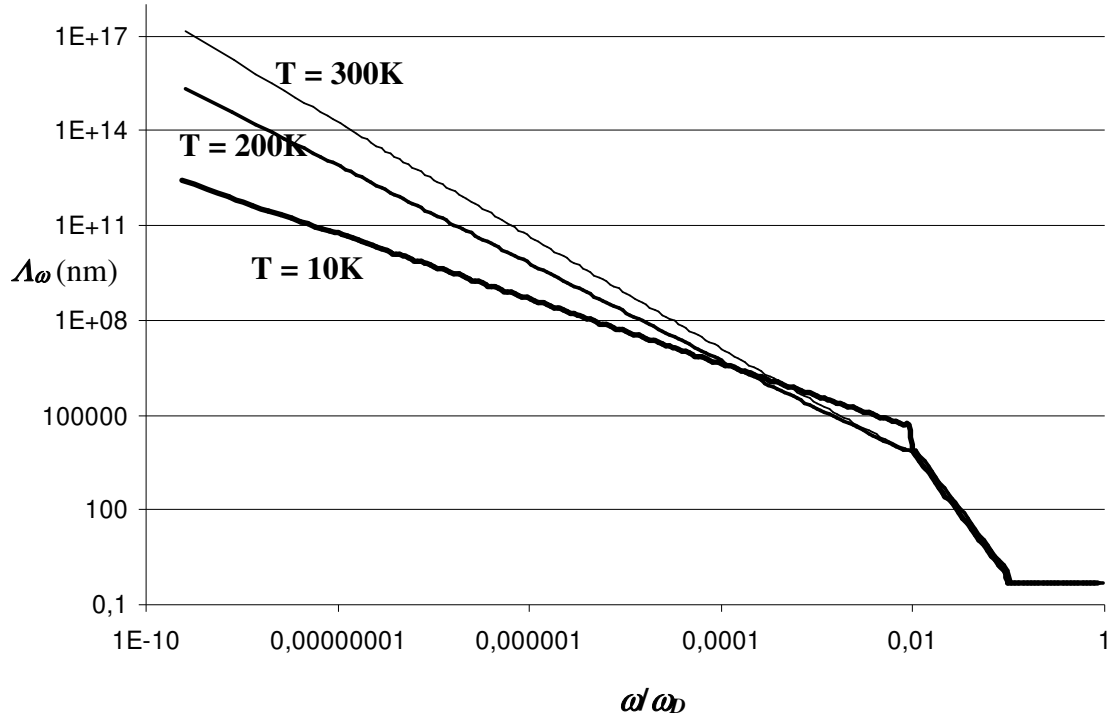


Figure 4: Evolution of the phonon mean free path in silica with frequency

The thermal conductivity of silica can be evaluated from the following formula already used by Kittel [10], Holland [34] and Berman [35]:

$$k = v_s \int_0^{\omega_D} C_s(\omega, T) \Lambda(\omega, T) h_p / (k_B \cdot T) d\omega \quad (3)$$

The thermal conductivity of silica calculated at different temperatures by this formula using the properties proposed by Goodson et al. have been compared with the experimental data obtained by Jund and Jullien [36] and Love and Anderson [27], the results are given on the following figure :

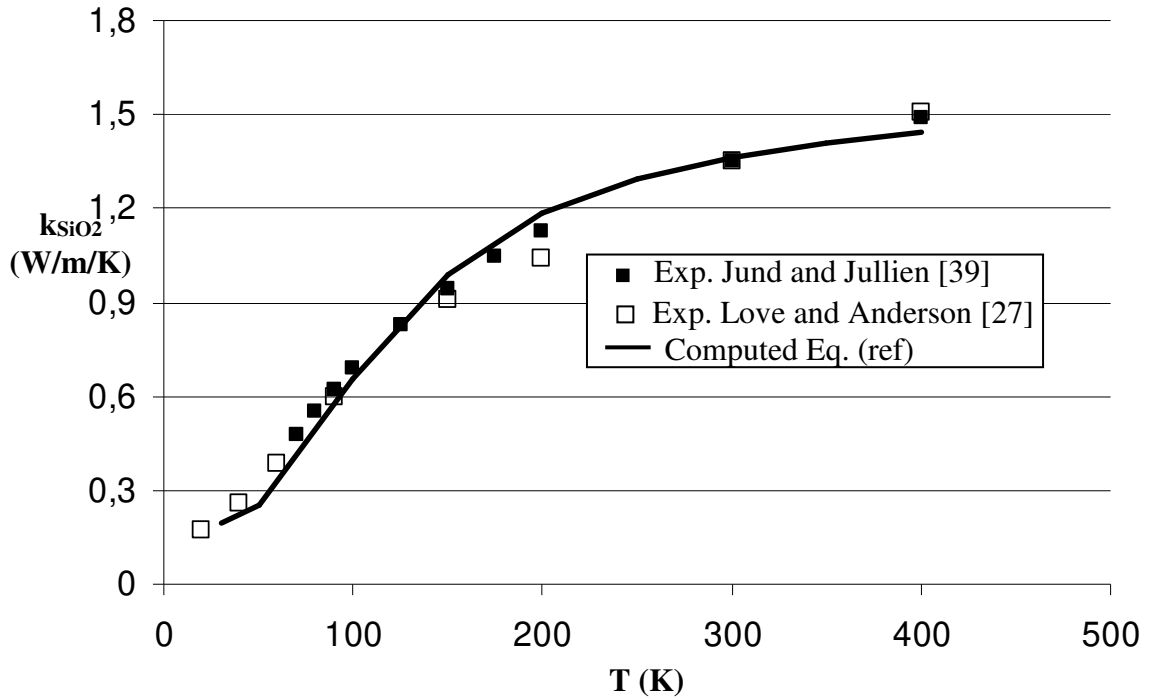


Figure 5: Evolution of the conductivity of silica with temperature predicted by the model of Goodson et al. [27]; comparison with experimental data

The agreement between the model results and the experimental data is satisfactory. For example, at 300 K both experimental values give $k_{\text{SiO}_2} = 1.35 \text{ W/m/K}$ and the model of Goodson leads to $k_{\text{SiO}_2} \approx 1.36 \text{ W/m/K}$. Moreover, the drop of the thermal conductivity of silica with temperature is well-reproduced by the model. Therefore, we will consider in the rest of the study that the phonon properties proposed by the model of Goodson et al. are sufficiently reliable to be used for the evaluation of the heat transfer through the solid phase at nanometric scale.

2.2.2 Modeling of $k_{p \rightarrow p}$ using MC simulation of phonon transport for the resolution of Boltzmann Equation

As explained in the introduction, the validity of the macroscopic Fourier laws for modeling conduction heat transfer between nano-particles is questionable as the particles dimensions are comparable with the phonon mean free path. It is then necessary to solve the Boltzmann Equation governing the distribution and transport of phonons in the material:

$$\frac{\partial \mathbf{n}_\omega(t, \vec{s})}{\partial t} + \vec{v}_s \cdot \vec{\nabla} \mathbf{n}_\omega(t, \vec{s}) = \left(\frac{\partial \mathbf{n}_\omega(t, \vec{s})}{\partial t} \right)_{coll} \quad (4)$$

with $\mathbf{n}_\omega(t, \vec{s})$ the phonon distribution function, \vec{v}_s the group velocity.

The terms in the left-hand side of Eq. (4) correspond to the total time rate of change of \mathbf{n}_ω and the diffusion in geometric space due to the phonon group velocity \vec{v}_s , while the right-hand side represents the rate of change of \mathbf{n}_ω due to phonons scattering because of impurities, collisions with boundaries or phonon-phonon scattering. The heat flux due to phonon transport is then given by:

$$\vec{q}(\vec{s}, t) = \int \mathbf{h}_p \cdot \omega \vec{v}_s \cdot \mathbf{n}(t, \vec{s}) \cdot D_p(\omega) d\omega \quad (5)$$

For the moment, the resolution of the Boltzmann Equation for heat transfer calculations has been applied essentially to silicon-based microelectronics components [14-20]. Monte Carlo simulations are generally used for the resolution of the Equation in complex structures due to their adaptability to various geometries. It has been used by Majumdar [14] for thin silicon films and more recently by Randrianalisoa and Baillis [20] to evaluate the thermal conductivity of nanoporous silicon films. It is particularly well-adapted to our problem. The method principle is to mimic numerically a guarded hot plate experiment applied to a particle-particle contact. The 3-D nanometric structure analysed is submitted to a 1-D temperature gradient between a hot (temperature T_h) and a cold (temperature T_c) plate (see Fig. 6). The nano-particles in contact are discretised in 3-D elementary cells, generally parallelepipedic, which are chosen to be smaller than the phonon mean free path in order to ensure that there is no more than one intrinsic scattering in a cell. The interface between solid and fluid phase are delimited. An arbitrary temperature (which is still to be determined) is affected to each elementary cell of the mesh. Thereafter, a procedure of phonon tracking is applied and allows adjusting the temperature field in the system until the steady-state regime is reached.

Phonons are emitted from the hot and cold boundaries which are assumed to behave as black walls with prescribed temperatures (T_h and T_c). The phonon flux Q^+ emitted from each plate is divided into very high number of phonon samples. Q^+ is related to the wall temperature through

$$Q^+(T) = A.v_s \int_0^{\omega_p} D_p(\omega, T).N(\omega, T).h_p.\omega d\omega \quad (6)$$

where $N(\omega, T) = \frac{1}{\exp(h_p.\omega/(k_B.T)) - 1}$ is the average number of phonons that occupy the vibration state of frequency ω at temperature T .

1. For every phonon emitted by the plates, random location, direction and frequency are chosen. Then, the procedure follows the path of the phonon. It propagates in the material in straight lines and can be reflected by the material boundaries between the solid and fluid phases. The phonon tracking is stopped when it is absorbed in an elementary cell or on one of the hot or cold plates. Each time a phonon is absorbed, the energy of the absorbing element (plate or cell) is incremented by the phonon sample energy. When the path of all the phonon samples emitted by the plates have been tracked, the energy absorbed by each element, noted Q_c^- and Q_f^- for the hot and cold boundaries and G_i^- for the cells is memorised.
2. Thereafter, from each cell i , a certain number of phonons are emitted so that the energy emitted by the cell, denoted by G_i^+ equals the cell absorbed energy G_i^- . These newly emitted phonons are tracked again one by one until they are all absorbed. After this phonon tracking, the energies absorbed at cells and walls only during this step, referred as “current energy”, are computed.

3. Finally, while the “current energy” absorbed at cells and walls are greater than zero, they are added to the absorbed energies Q_c^- and Q_f^- for walls and G_i^- for cells, and the algorithm goes back to step 2. Since the phonons absorbed at the boundaries are not reintroduced, the total phonon number in the studied system decreases step by step and becomes equal to zero after a certain number of steps. In practice, the procedure stops when the energy of the remaining phonons are considered negligible. The temperature field in the structure and the net energy flux crossing the material may be extracted from the energies emitted (Q_c^+ , Q_f^+ and G_i^+) and absorbed (Q_c^- , Q_f^- and G_i^-) by each element. Indeed, in steady-state regime, the energy emitted and absorbed by each cell are equal to

$$G_i = V_i \int_0^{\omega_p} \frac{1}{\tau_\omega} D_p(\omega, T_i) N(\omega, T_i) h_p \cdot \omega d\omega \quad (7)$$

Thus, the temperature of each element can be determined by simply inverting the preceding relation for satisfying the relation $G_i = G_i^-$.

As the initial temperature field is allocated arbitrarily, the distribution of phonon frequency in each cell is not correct and the temperature field computed at the end of the procedure is different from the initial field. Therefore, iterations are required and steps 1-3 are repeated until the temperature field is stable, i.e. practically invariant for two consecutive iteration level.

The Monte Carlo procedure is summarized by the flowchart depicted on Fig. 7.

When the steady-state is reached, the particle-particle thermal conductivity $k_{p \rightarrow p}$ can be calculated from the net heat flux Q crossing the two particles:

$$k_{p \rightarrow p} = \frac{1}{A} \left| \frac{Q}{\Delta T / \Delta z} \right| = \frac{1}{\pi \cdot D_p^2 / 4} \left| \frac{Q}{(T_h - T_c) / l} \right| \quad (8)$$

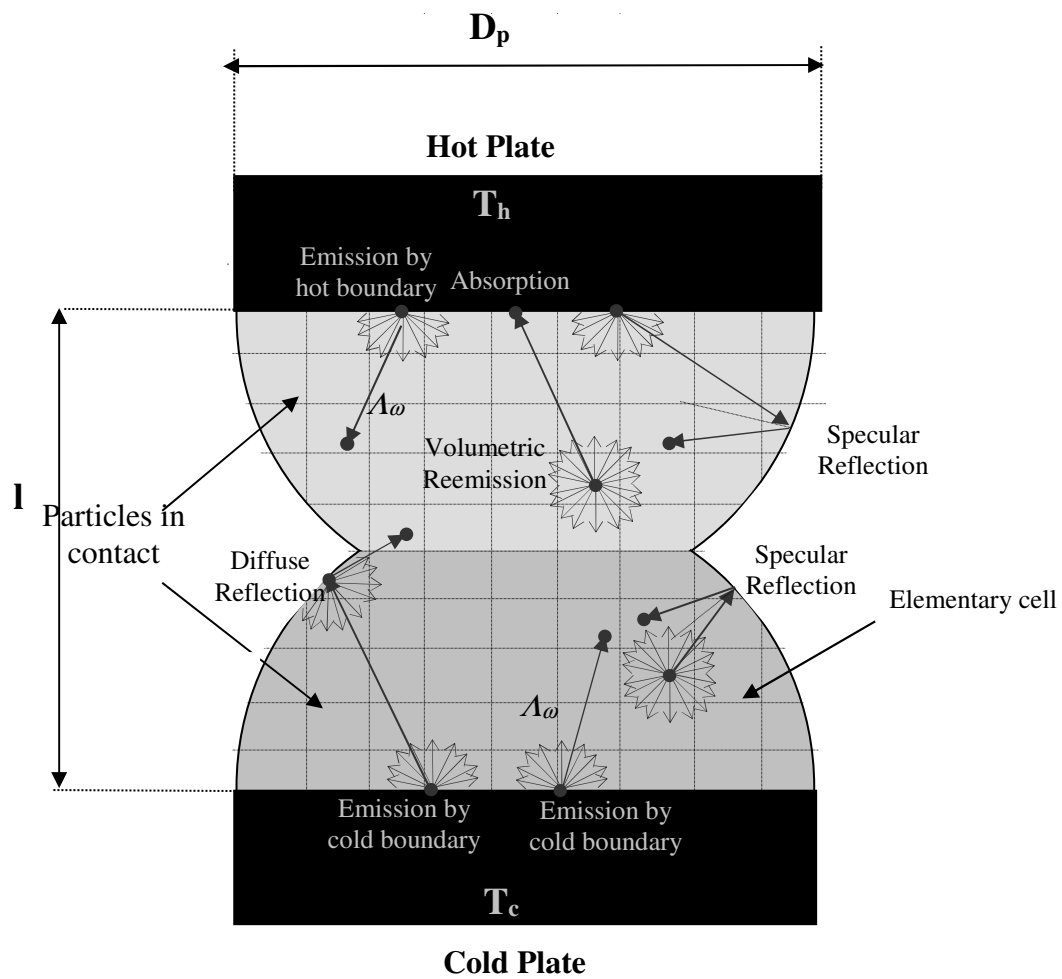


Figure 6: Illustration of the Monte Carlo procedure for the resolution of Boltzmann Equation for two nano-particles in contact

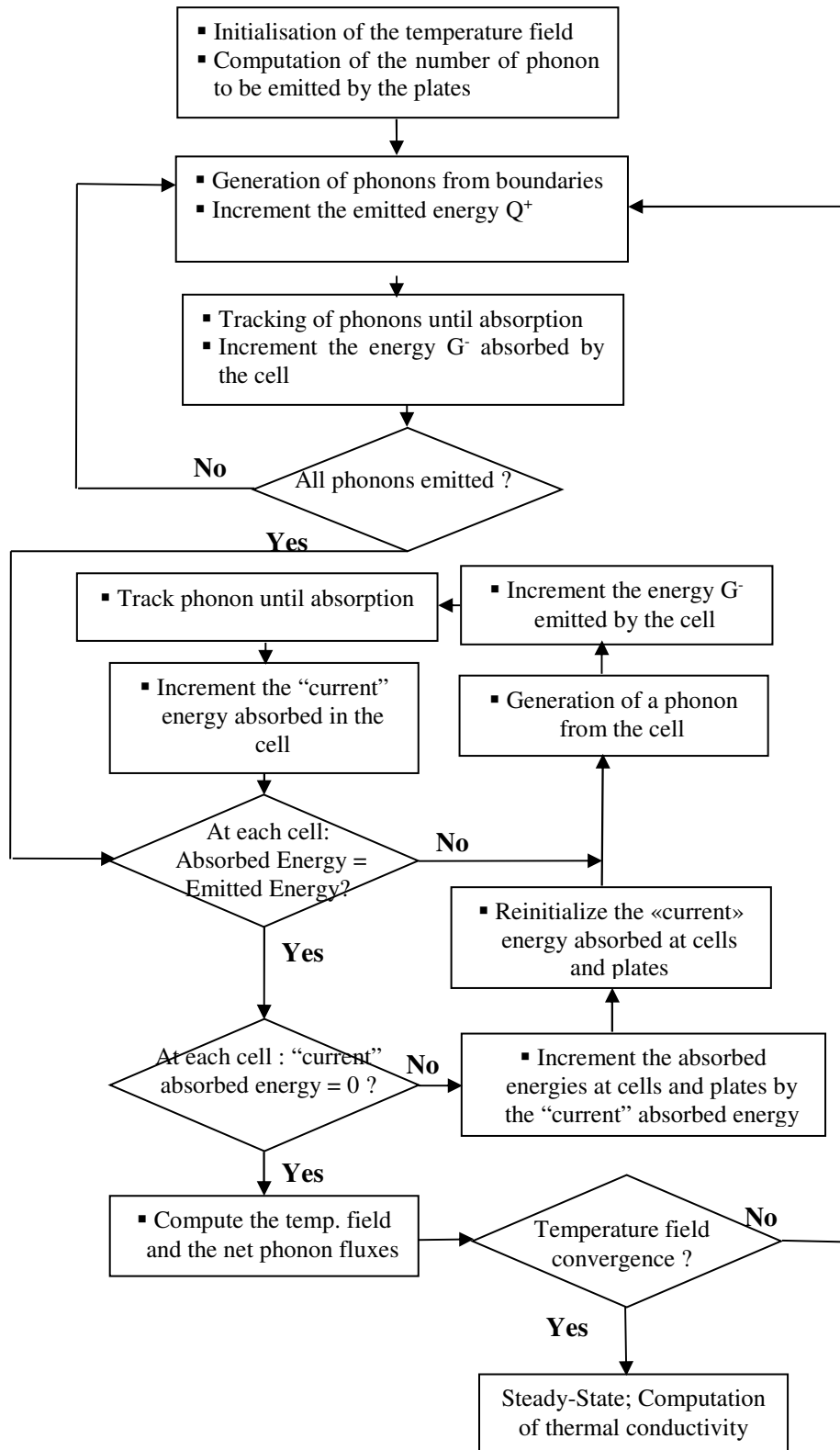


Figure 7: Flow-chart of the Monte Carlo procedure used for the resolution of Boltzmann Equation in the nano-structure

2.3 Modeling of the heat exchange inside the agglomerated structure

2.3.1 Finite Volume Method

Once the heat exchange between two silica nano-particles in contact has been computed using the approach presented in section 2.2, the effective thermal conductivity of the global material should be evaluated by considering its microscopic structure formed by the agglomeration of aggregates. The first step is to generate a volume filled, by the tangle of spherical nano-particles aggregates, which is representative of the silica-based nano-structured material. This parallelepipedic volume must have given geometrical characteristics (particles size, global porosity, aggregates fractal characteristics). Thereafter, the effective thermal conductivity of this “cloud” of aggregates is computed by a Finite Volume Method (FVM) simulating numerically a 1-D temperature gradient applied to the volume generated along the z-axis (see Fig. 8). The developed model computes the temperature field inside each particle and the total heat flux passing through the material in steady-state regime. The resolution method uses an iterative process based on an energy balance on each particle whose temperature is considered homogeneous. The computation starts from an initial temperature field. For each nano-particle of the volume, the procedure computes the heat exchanged with the neighboring particles in contact and with the surrounding fluid phase. The energy balance is then used to correct the temperature field of the previous iteration level. The energy balance and the correction of the temperature field are repeated until the steady-state regime is reached, i.e. until the temperature of each particle is stable from one iteration level to another.

In practice, the initial temperature field is assumed to vary linearly with z:

$$T_k^0 = \frac{T_c \times z_k}{L} + \frac{T_f \times (L - z_k)}{L} \quad (9)$$

The heat fluxes exchanged by the neighbouring nano-particles depend on the particle-particle conductivity $k_{p \rightarrow p}$ determined previously as well as on the temperature gradient between the

centres of these particles. The heat flux exchanged by particle k (Temperature T_k) with its n^{th} neighbour (Temperature $T_{k,n}$) is given by:

$$\dot{Q}_{k,n} = k_{p \rightarrow p} \cdot A \cdot \frac{\partial T}{\partial s} \Rightarrow \dot{Q}_{k,n} = k_{p \rightarrow p} \cdot \frac{\pi \cdot D_p^2}{4} \cdot \frac{T_{k,n} - T_k}{\Delta s_n} \quad (10)$$

with Δs_n the distance between the centres of the two nano-particles

However, we will see in the next that the formation process of nano-structured silica-based materials leads to two different types of links between two particles in contact. Thus, we set apart:

1. the links created between two particles of a common aggregate during its formation in the flame, noted “intra-aggregate” links
2. the particle-particle links that have been established during the compression of the arrangement of aggregates between two particles of different aggregates, noted “inter-aggregate” contacts

As explained in the introduction, the “intra-aggregate” links formed in the flame (Wan der Waals links) are known to be undividable and therefore stronger than the “inter-aggregate” links (links by physical forces) which are obtained by a simple contact during the compression. Therefore, the particle-particle conductivity $k_{p \rightarrow p}$ may be noticeably different according to the link type; we distinguished in our computations the “intra-aggregate” value denoted $k_{p \rightarrow p,1}$ and the “inter-aggregate” value denoted $k_{p \rightarrow p,2}$.

N.B.: Considering the previous observations, it is obvious that $k_{p \rightarrow p,2}$ is always lower or, in the best case, equal to $k_{p \rightarrow p,1}$.

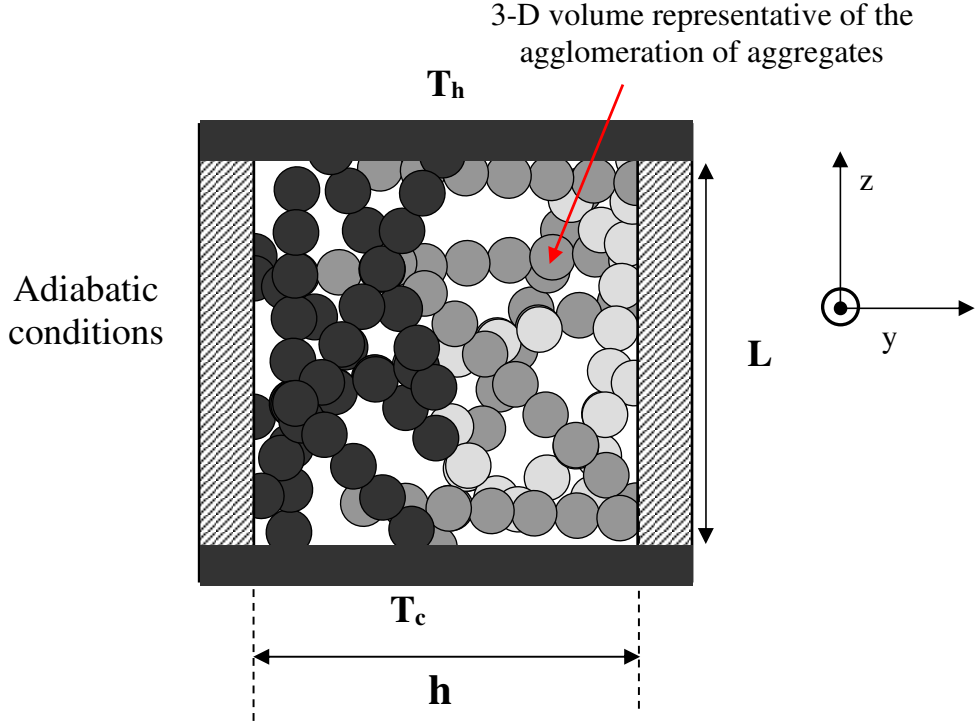


Figure 8: Principle of the effective thermal conductivity computation for arrangement of aggregates of nano-particles using FVM

The nano-particle may also exchange with the surrounding fluid. However, according to previous studies, heat-transfer fluxes at the interface of a solid surface and a rarefied gas can be neglected. Indeed, Demirel and Saxenas [37] have proposed analytical formulas to estimate these heat fluxes for different heat transfer regimes characterised by interval values of the Knudsen number $Kn = L_g / t_p$. Nano-structured silicas submitted to a partial vacuum (10 mbar for example) lie in the free-molecule heat-conduction regime ($Kn > 10$). Then, the heat exchange coefficient between two parallel plates (1 and 2) reflecting the gas molecule diffusely is given by

$$h_{FM} = \left[\frac{1}{\alpha_1} + \left(\frac{1}{\alpha_2} - 1 \right) \right]^{-1} \frac{P(C_v + R/2)}{2\pi \cdot R \cdot T^* \cdot M_g} \quad (11)$$

$$\text{with } T^* = \left(\frac{1}{2} \left(\frac{1}{\sqrt{T_{r1}^*}} \right) + \frac{1}{2} \left(\frac{1}{\sqrt{T_{r2}^*}} \right) \right); \quad T_{r1}^* = \frac{\alpha_1 \cdot (1 - (1 - \alpha_2)) T_1 + \alpha_2 (1 - \alpha_1) T_2}{(1 - (1 - \alpha_1) \cdot (1 - \alpha_2))};$$

$$T_{r2}^* = \frac{\alpha_2 \cdot (1 - (1 - \alpha_1)) T_2 + \alpha_1 (1 - \alpha_2) T_1}{(1 - (1 - \alpha_2) \cdot (1 - \alpha_1))};$$

where P the pressure ; C_v the molar heat capacity; M_g the molecular weight of the gas, R the molar gas constant and α₁ and α₂ the coefficients of accommodation measuring the efficiency of energy exchange between the gas stream and the solid surface.

This heat exchange coefficient is maximal when α₁=α₂ and is approximately h_{FM} = 55 W/m²/K for heat exchange in air (C_v = 20.8 J/K/mol; M_g = 0.02897 kg/mol) at P=10 mbar between parallel plates with temperatures near 300K. We will see in the next that this value is quite negligible compared to the heat flux exchanged between two neighbouring particles in contact. Of course, the parallel-plates geometry is noticeably different from the geometry encountered in nano-structured silicas but it permits to approximate the order of magnitude. Therefore, in the light of the preceding considering, we will neglect the exchange between particles and fluid in the rest of the study.

The adjustment of the temperature of particle k at each iteration, takes inspiration from the transient Energy Equation:

$$\rho \cdot C_p \cdot V_k \cdot \frac{\partial T_k}{\partial t} = \sum_{n=1}^N \dot{Q}_{k,n} \Rightarrow \frac{\rho \cdot C_p \cdot V_k}{\Delta t} \cdot (T_k^{i+1} - T_k^i) = \sum_{n=1}^N \dot{Q}_{k,n} \Rightarrow T_k^{i+1} = T_k^i + C \cdot \sum_{n=1}^N \dot{Q}_{k,n} \quad (12)$$

with N the number of particles in contact with particle k

The energy balance and the correction of the temperature field in the nano-particles are repeated until convergence, i.e. until the following criterion is satisfied:

$$\frac{|T_k^{i+1} - T_k^i|}{T_k^i} < \xi \quad \forall k \quad (13)$$

The value of the constant parameter C is adjusted so that the convergence is achieved in a minimum number of iterations.

Regarding the fluid phase, given that the fluid-solid exchange can be considered negligible, we could assume that the temperature of the fluid phase in steady-state is governed by:

$$\frac{\partial \left(k_f \cdot \frac{\partial T_f}{\partial z} \right)}{\partial z} = 0 \Leftrightarrow k_f \cdot \frac{\partial T_f}{\partial z} = C^{ste} \quad (14)$$

with k_f given by the relation for confined gas (Eq. (1))

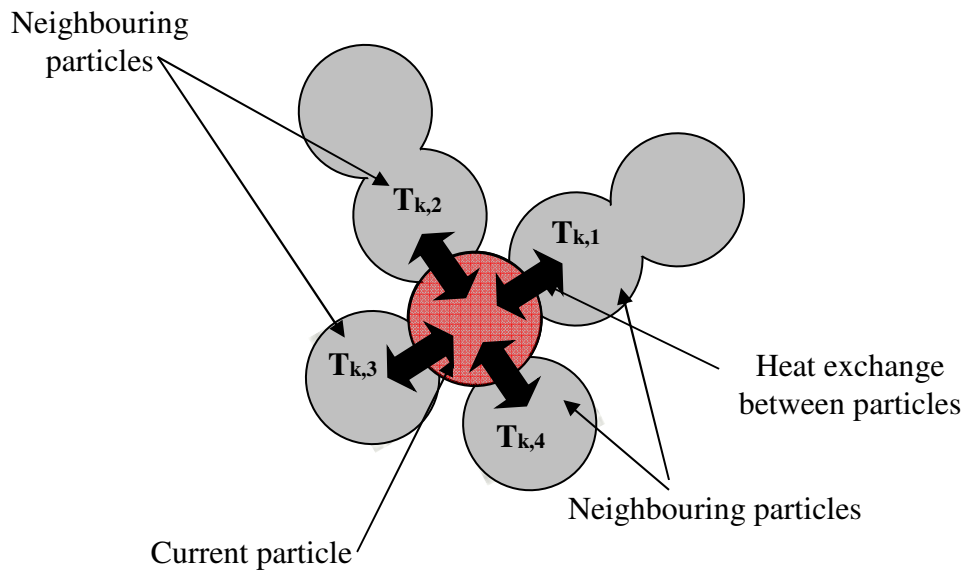


Figure 9: 2-D Illustration of the thermal balance during the Finite Volume computation

Therefore, if the temperature difference between the hot and cold plates is small enough to neglect the variations of the fluid phase conductivity between hot and cold boundaries, the temperature field in the fluid phase varies linearly with z :

$$T_{f,z} = \frac{T_{hot} \times z}{L} + \frac{T_{cold} \times (L - z)}{L} \quad (15)$$

Once the temperature field in the nano-particles and in the gas phase have been determined, the effective thermal conductivity of the material in the z direction can be computed from the heat flux \dot{Q}_z crossing parallel planes (x,y) at different height Z through the solid and gas phase. In steady-state, these heat fluxes are invariant with Z . They are evaluated by summing

the contributions of each nano-particle exchanging with a particle located across the (x,y) plane and the contribution of the heat transfer through the fluid phase as well. The effective thermal conductivity is then given by:

$$\dot{Q}_z = k_{eff} h^2 \frac{(T_{hot} - T_{cold})}{L} \Leftrightarrow k_{eff} = \frac{\dot{Q}_z \cdot L}{(T_{hot} - T_{cold}) h^2} \quad (16)$$

2.3.2 Generation of volumes representative of the nano-structured silicas

The Finite Volume computations must be applied to samples representative of the microscopic structure of the material. The data required for the computation are simply the coordinates of the center of each particle forming the sample, their diameter as well as the list of the particles in contact and the type of links (“intra-aggregate” or “inter-aggregate”). These parallelepiped representative volumes, whose dimensions must be large enough, have been generated by imitating numerically the phenomena occurring during the formation of the nano-structured silicas:

1. An initial Fractal-like aggregate is first generated using the Sequential Algorithm (SA) described by Mackovski [24] (see section 2.1) and randomly placed in the parallelepipedic box by randomly choosing its location and orientation.
2. Additional aggregates different from the initial one but having the same fractal characteristics D_f , k_0 and N_p are then generated and also placed randomly in the box. Of course, they are not allowed to overlap the aggregates already placed. These new aggregates are not necessarily entirely comprised in the parallelepipedic volume: some of its particles can be outside. However, only the particles inside the volume will be taken into account. For each particle, the neighbouring particles belonging to the same aggregates are memorised.
3. Step 2 is repeated until it is not possible to insert additional aggregate

The media generated by this procedure have a porosity generally comprised between 0.96 and 0.93, i.e. noticeably more important than that of nano-structured silicas used in commercially available VIPs. Indeed, they are generally compressed to obtain a sufficient mechanical resistance. This compression is simulated numerically by reducing progressively the dimensions of the parallelepipedic box. Each particle getting in contact with the boundaries of the box are moved as well as its neighbours. Therefore, the arrangement of particles is redistributed at each compression step by keeping the undividable links inside a given aggregate invariant. During the compression process, certain particles can encounter particles belonging to other aggregates. In this case, the procedure put a thermal contact between the two particles and the particles are related by an “inter-aggregate” link. As explained before, this thermal contact is of different nature from the undividable link between neighbouring particles belonging to a given aggregate. Finally, the compression procedure allows obtaining arrangements with porosity close to 0.8.

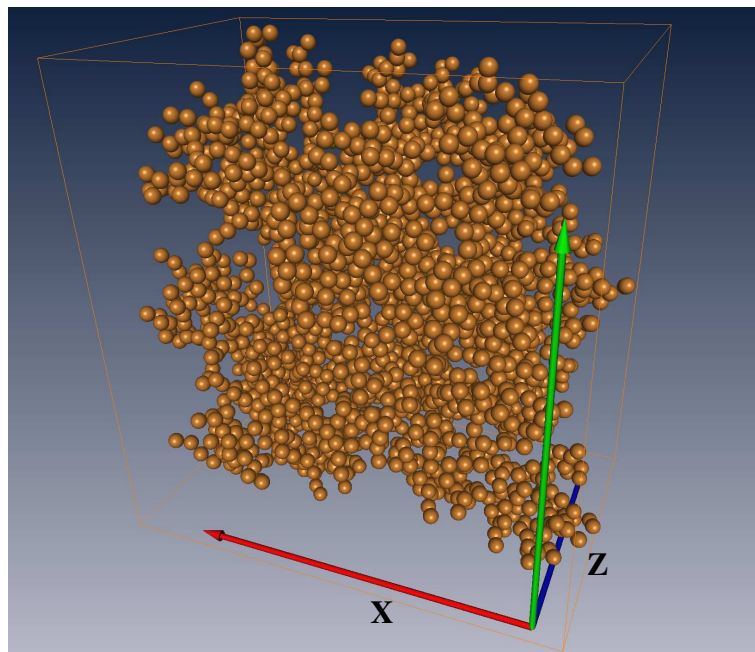


Figure 10: Illustration of a parallelepipedic volume representative of a fractal aggregates arrangement

2.3.3 Characteristic pores size

The pores dimension t_p is a main characteristic of the nano-structured material, because it affects directly the reduction of fluid phase conductivity due to the “Knudsen effect” according to Eq. (1). Thus, for each generated arrangement, this characteristic size has been estimated. Actually, it corresponds to the mean distance travelled by a gas molecule between two successive collisions with the solid phase. This size depends on the porosity ε , the particle diameter D_p but also on the fractal characteristics of the aggregates (D_f , k_0 , N_p). We have evaluated it numerically using a method inspired from ray-tracing procedures. The path of air molecules is analysed during their multiple collisions with the particles forming the representative volume and the mean distance travelled between two collisions is evaluated for a high number of molecules thrown. The results obtained for representative volumes generated with different fractal characteristics, are illustrated on Fig. 11 where we depict the evolution of the ratio t_p/D_p as a function of the solid fraction.

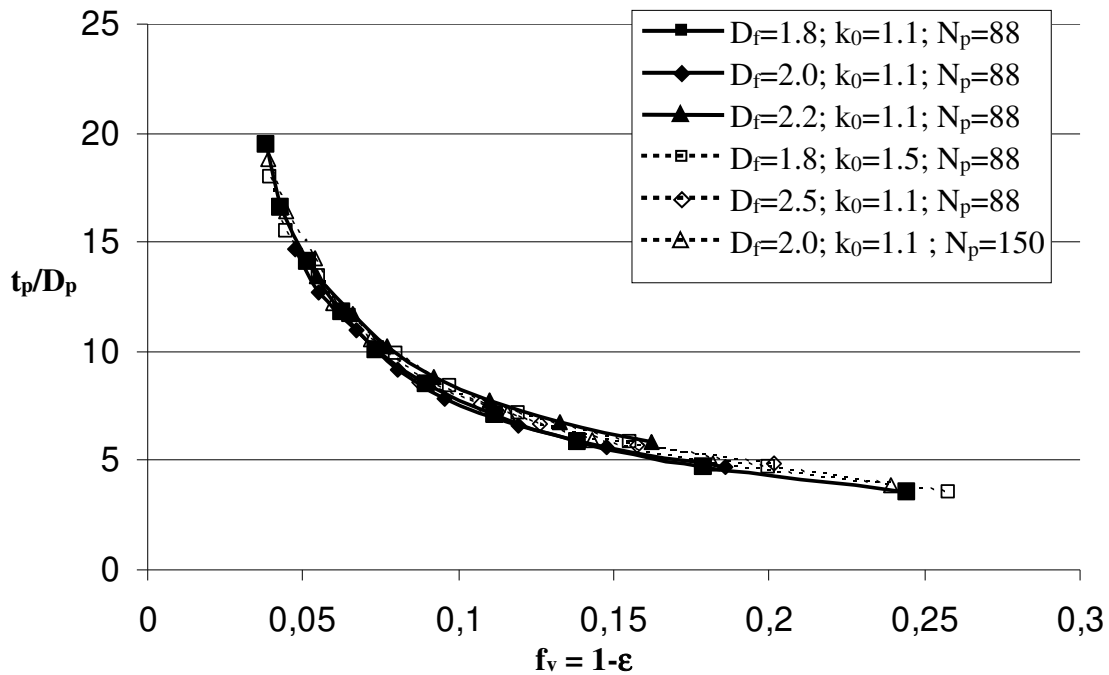


Figure 11: Evolution of the pore characteristic size with the solid fraction in arrangement of aggregates with different fractal characteristics

One can remark that there are relatively small differences between the evolutions of the characteristic pore dimensions computed for arrangements with different fractal characteristics of aggregates. From these evolutions, we can compute the thermal conductivity of the confined air for the different types of arrangement using Eq. (1).

3 Results

3.1 Nanometric scale – Variations of the particle-particle conductivity

We have applied the resolution of the Boltzmann Equation using Monte Carlo simulations for particle-particle junctions with varying geometrical characteristics D_p and D_c/D_p using the phonon properties given by the model of Goodson et al. at a temperature of 290 K. The main results are illustrated on the following figures for two different values of contact diameters: $D_c \approx 0.44 \times D_p$ and $D_c \approx 0.66 \times D_p$. On the same figure, we have also illustrated the particle-particle thermal conductivity that would be obtained if the macroscopic Fourier law was valid. These values are, of course, independent of the particles diameter D_p . They have been obtained by solving the Energy Equation using a Finite Volume Method in the same geometry as the one illustrated on Fig. 6. The Equation and the corresponding boundary conditions are

$$\frac{\partial}{\partial x} \left(\mathbf{k}_x \frac{\partial T}{\partial x} \right) + \frac{\partial}{\partial y} \left(\mathbf{k}_y \frac{\partial T}{\partial y} \right) + \frac{\partial}{\partial z} \left(\mathbf{k}_z \frac{\partial T}{\partial z} \right) = 0 \quad (17)$$

$$T_{z=0} = T_h, T_{z=l} = T_c, \left(\frac{\partial T}{\partial x} \right)_{x=0} = 0, \left(\frac{\partial T}{\partial x} \right)_{x=D_p} = 0, \left(\frac{\partial T}{\partial y} \right)_{y=0} = 0, \left(\frac{\partial T}{\partial y} \right)_{y=D_p} = 0$$

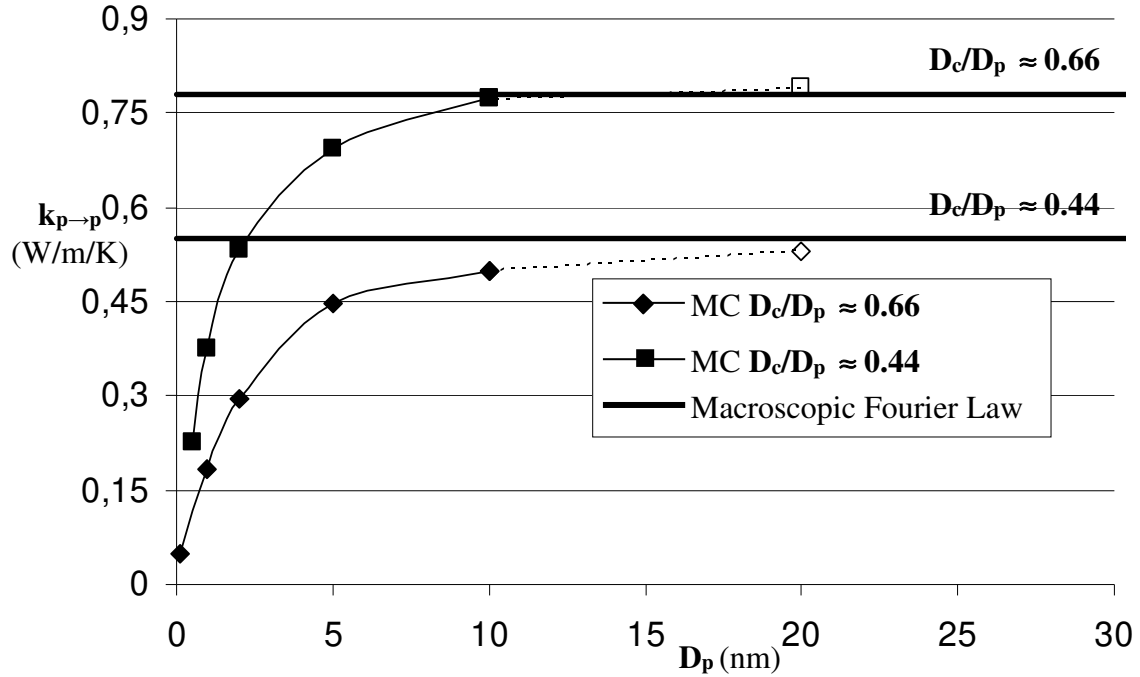


Figure 12: Evolution of the particle-particle conductivity with the particle diameter for different contact area D_c/D_p

The FVM computations were conducted by setting the thermal conductivities of the solid phases to the macroscopic conductivity of silica ($k_x=k_y=k_z=k_{SiO_2}$) while the thermal conductivity of air was set to a very low value.

The results obtained show that the “nanoscopic effects” evocated in the introduction really affect the thermal conductivity for particle diameters D_p lower than about 10 nm. The particle-particle conductivity decreases more and more rapidly when D_p diminishes below 5 nm. On the other hand, for $D_p > 10$ nm, $k_{p \to p}$ converges to the value obtained under the “macroscopic” assumption. However, it is important to note that it was not possible to conduct the resolution of Boltzmann equation, using the Monte Carlo approach for particles diameters above 20 nm, given that the memory resource required for the proper particles meshing exceeds our computers capacities. Indeed, as explained in section 2.2.2, the characteristic size of the discretization volume must remain lower than the phonon mean free paths (approximately 0.5 nm in our case). Besides, the values of $k_{p \to p}$ illustrated for $D_p = 20$ nm have to be considered with caution given that the preceding condition is not fully fulfilled. That is the reason why

the curve between $D_p=10$ nm and $D_p=20$ nm are illustrated by dotted lines. However, this does not put in question the preceding conclusions concerning the convergence of the MC computations when D_p becomes sufficiently important. Another interesting remark concerns the strong influence of the contact area between the particles on the intensity of the heat exchange. This influence is illustrated on Fig. 12, where we have depicted the variations of $k_{p \rightarrow p}$ with the ratio D_c/D_p obtained by solving the Boltzmann Equation using MC approaches for $D_p=5$ nm and $D_p=10$ nm. On the same figure, we have also represented the variations obtained when assuming that the macroscopic Fourier laws are valid.

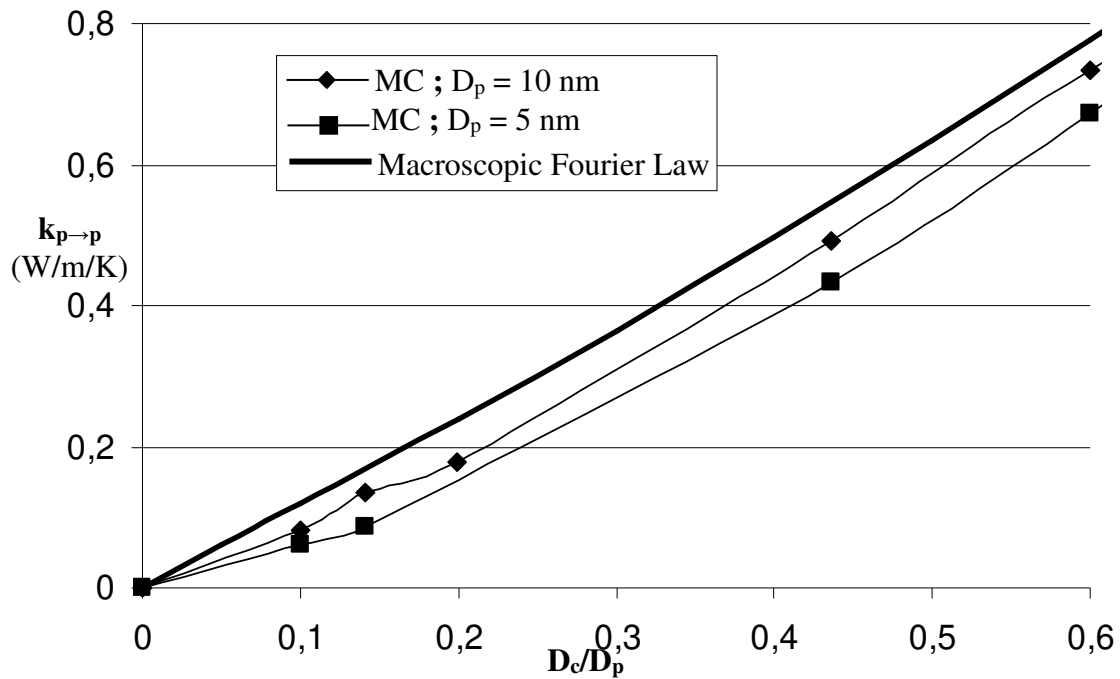


Figure 13: Evolution of the $k_{p \rightarrow p}$ with the ratio D_c/D_p computed using MC simulations for the resolution of Boltzmann Equation or using the Macroscopic Fourier laws

It is interesting to notice that the profile of the evolutions computed by solving the Boltzmann Equation via MC simulations or by using the macroscopic law of heat conduction, are very similar. Only the magnitude of heat exchange differs slightly. Actually, the “nanoscopic” effects tend to reduce $k_{p \rightarrow p}$ and thus, its value gets lower when the particle diameter decreases

below 10 nm. In addition, one can check that, in all cases, the heat exchange gets null when the contact between the two particles gets close to a point contact.

In the light of these results, it appears that the contact area between the particles is the key-parameter that mostly governs the magnitude of heat exchange, even more than the particle diameter. In order to obtain realistic estimations, it is therefore essential to know this parameter with a high degree of confidence for both “intra-aggregate” and “inter-aggregate” contacts. Finally, one can notice that $k_{p \rightarrow p}$ varies approximately in the range $[0, 0.6]$ W/m/K when D_c/D_p varies between 0 and 0.5.

3.2 Microscopic scale – Parametric study

The preceding sections have analysed the heat transfer mechanisms at nanometric and microscopic scale; this allowed us to highlight the structural characteristics and thermo-physical properties influencing significantly the heat exchange in nano-structured silica-based materials. The identified parameters are:

- At nanometric scale : particle diameter D_p , and contact area $(D_c/D_p)_1$ between particles in contact inside a given aggregate (“intra-aggregate” link)
- At microscopic scale (agglomerate of aggregates): confined gas pressure P of, density ρ , aggregates fractal characteristics (D_f , k_0 , and N_p), contact area $(D_c/D_p)_2$ between particles put in contact during the compression (“inter-aggregate” link).

In order to quantify the influence of these parameters, we have conducted a parametric study by varying their values around standard values: $D_p=10$ nm ; $(D_c/D_p)_1 = (D_c/D_p)_2 = 0.2$ leading to $k_{p \rightarrow p,1} = k_{p \rightarrow p,2} \approx 0.18$ W/m/K; $P=10$ mbar ; $\rho=300$ kg/m³; and $D_f = 2.0$, $k_0=1.1$, and $N_p=88$ (see [22, 23]).

3.2.1 Influence of the density

The computation model of effective thermal conductivity, described in section 2.3.1 has been applied to several parallelepipedic volumes representative of a fractal-like aggregates arrangement. We have varied the compression rate for varying the density of the aggregates arrangements representative of nano-structured silicas in the range [100, 600] kg/m³. First, the computations have been conducted assuming that the thermal contacts between particles are all identical: $k_{p \rightarrow p,1} = k_{p \rightarrow p,2}$. We have also set $D_p = 10$ nm, $P = 10$ mbar and $D_c/D_p = 0.2$ which leads to $k_{p \rightarrow p,1} = k_{p \rightarrow p,2} \approx 0.18$ W/m/K. The evolutions of the computed effective conductivities as a function of material density are illustrated on Fig. 14. We have set the bulk silica density at $\rho_{SiO_2} = 2300$ kg/m³.

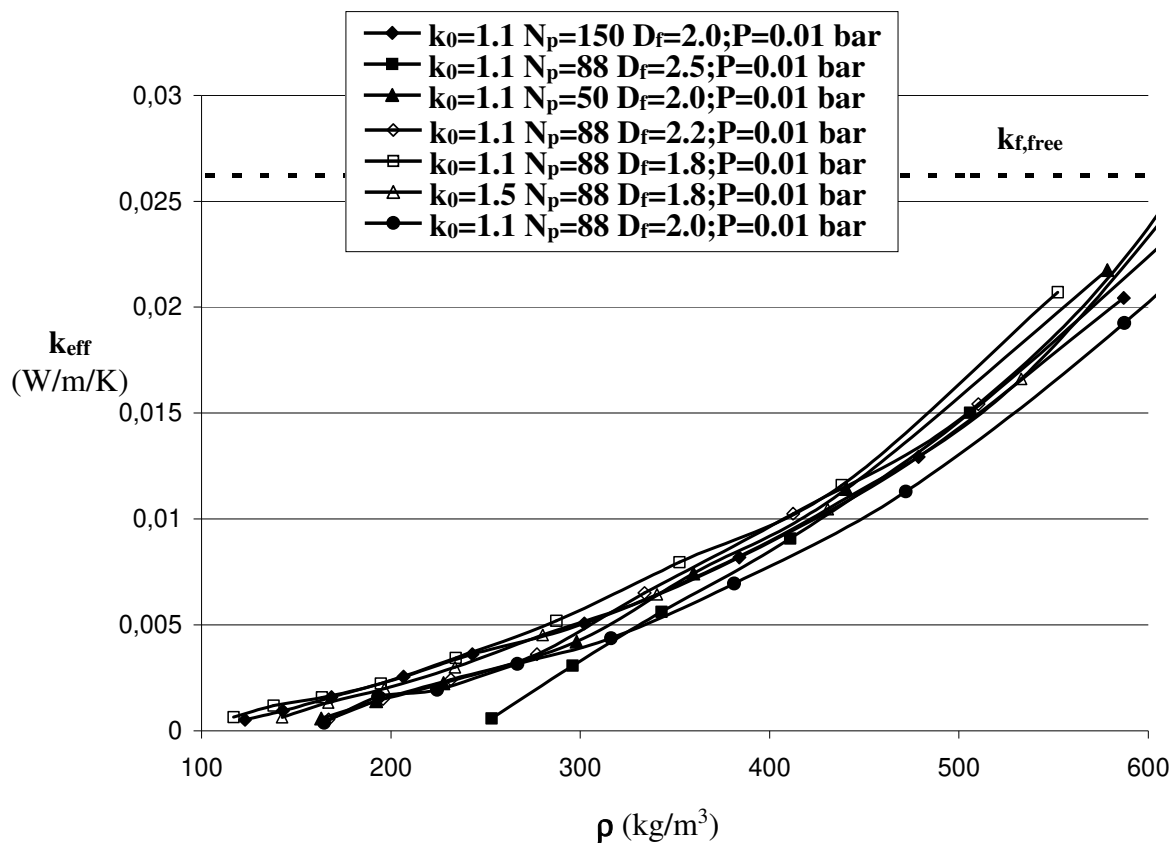


Figure 14: Evolution of the effective conductivity with density for arrangements of aggregates with different fractal characteristics and $D_c/D_p=0.2$ ($k_{p \rightarrow p,1} = k_{p \rightarrow p,2} \approx 0.18$ W/m/K)

First, one can notice that the effective thermal conductivities computed for a partial vacuum of 10 mbar and densities of about 300kg/m³ are significantly beyond the conductivity of free air at atmospheric pressure, whatever the fractal characteristics of the aggregates forming the arrangement. Indeed, the contribution of the confined fluid phase is then almost negligible even for relatively low densities for which the pore characteristic size is the most important. One can also remark that the effective thermal conductivities of the arrangements increase with density. This increase is due to the establishment of additional particle-particle contacts (“interparticle” contacts) during the compression and is not linear with ρ but almost quadratic. However, we have to keep in mind that the previous results were obtained assuming that inter-aggregate contacts may exchange as much heat as intra-aggregate ones. We will see in the next that the evolution may be different when the considered “inter-aggregate” heat exchange is weaker than the “intra-aggregate” one.

3.2.2 Influence of particle diameter

We have shown in section 3.1 that if particle diameter is lower than about 20nm, it may have a noticeable influence on the particle-particle conductivity. Indeed, the “nanoscopic effects” tend to reduce the heat exchange since the phonon mean free path in the material is affected/reduced by the presence of physical boundaries at nanometric scale. Moreover, the particle diameter also affects the characteristic pore size (see section 2.3.3) and thus the thermal conductivity of the confined gas. Actually, arrangements of agglomerates formed by large particles lead to higher values of t_p and k_{fluid} . We have illustrated the global influence of this parameter on the effective conductivity by varying the particle diameter while keeping the other parameters unchanged. The fractal characteristics of the aggregates have been set to standard values given by Lallich et al. [22, 23] : $D_f=1.8$; $k_0=1.1$, $N_p=88$.

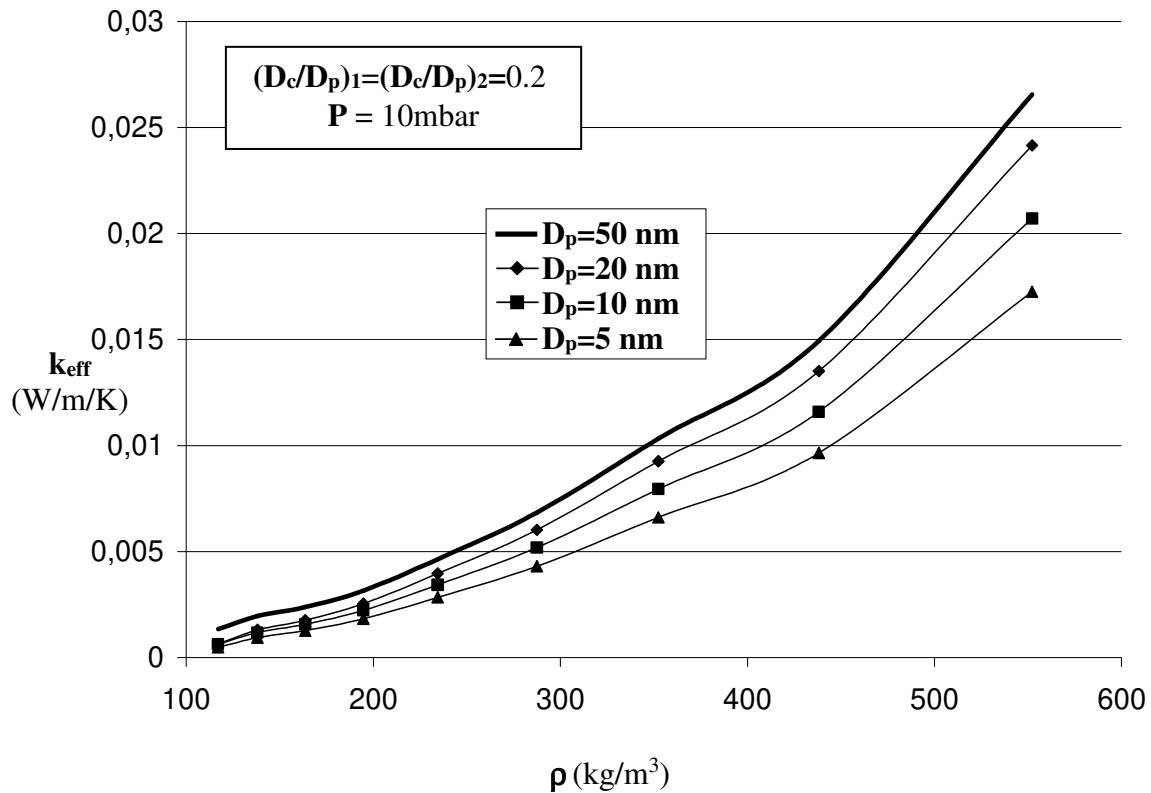


Figure 15: Evolution of the effective conductivity with density as a function of particle diameter for an arrangement of aggregates with $D_f=1.8$; $k_0=1.1$, $N_p=88$

One can remark that at low densities, such as non-compressed arrangement, the observed differences are relatively low and are almost entirely due to the differences in the confined fluid phase conductivity. When compression rate and density are increased, the differences between the evolutions for the different D_p increase. Now, nano-structured silicas commonly used in VIPs are made of particles with homogeneous diameters generally greater than 10 nm for which the “nanoscopic effects” are limited. Therefore, the influence of this parameter is in fact relatively limited.

3.2.3 Influence of contact areas between neighboring particles

The preceding results have been obtained using a ratio between contact diameter and particle diameter of $D_c/D_p=0.2$. Moreover, we have always assumed that the particles getting in contact during the compression (inter-aggregate) can exchange heat with the same magnitude as the particles in contact by undividable links inside a same aggregate (intra-

aggregates). In reality, the “inter-aggregate” heat exchange is most probably weaker than the “intra-aggregate”. Therefore, in order to account for this differentiation, we have conducted the computations for the same representative volume but affecting a particle-particle conductivity $k_{p \rightarrow p,2}$ noticeably lower than the inter-aggregates one. The results are illustrated on Fig. 16 for $(D_c/D_p)_2 = 0$ ($k_{p \rightarrow p,2} = 0$ W/m/K) and $(D_c/D_p)_2 = 0.05$ ($k_{p \rightarrow p,2} \approx 0.07$ W/m/K $\approx 0.4 \times k_{p \rightarrow p,1}$); the particle-particle conductivity for “intra-particle” contact is again set to $k_{p \rightarrow p,1} = 0.18$ W/m/K ($(D_c/D_p)_1 \approx 0.2$).

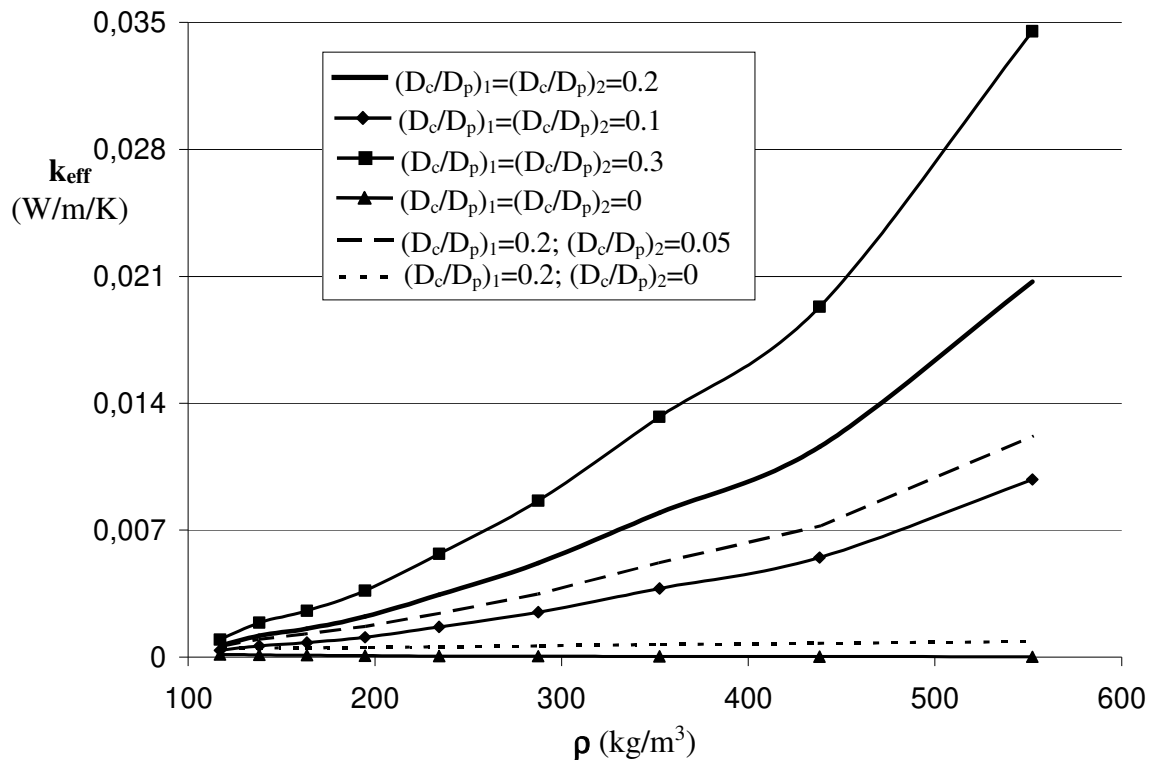


Figure 16: Influence of the contact areas on the evolution of the effective conductivity for an arrangement of aggregates with $D_i=1.8$; $k_0=1.1$, $N_p=88$ and $P=10$ mbar

As expected, the size of the contact area between particles in contact is a key-parameter that dictates the magnitude of conduction heat transfer in nano-structured silica-based materials. Large contact areas enhance the heat transport significantly. The higher the density, the stronger that effect is. The graphs in Fig. 16 also demonstrate that taking into account different values for “inter-particle” contact and “intra-particle” one impacts very strongly the effective conductivity. Indeed, when we assume that particles getting in contact

during the compression can exchange heat but less than the ones in “intra-particle” contact, the effective conductivity still increases with density but much more slowly. Now, for the extreme case of “inter-aggregate” contacts modelled as point contacts ($(D_c/D_p)_2=0$, no heat exchange), the effective conductivity of the material keeps almost constant even for high compression levels . In such a case the effective conductivity of the material is due only to conduction through the fluid phase. Indeed, the heat could not propagate only by particle-particle contact from one boundary to another, as the thermal exchange between aggregates is null and the aggregates size is too small to establish a direct thermal contact. We suppose that the thermal behaviour of the compressed arrangement is intermediate.

As a conclusion, it appears that precise modelling of heat transfer through nano-structured silicas requires real values of “intra-aggregate” and “inter-aggregate” contacts. .

3.2.4 Influence of the pressure of the confined gas

The very low thermal conductivity of nano-structured silicas is mainly due to the partial vacuum applied to the gas since it significantly reduces the confined fluid phase conductivity. However, for durability purpose, the partial vacuum may be not too high, since maintaining high vacuum for a long time is quite difficult. Therefore, it is interesting to evaluate the partial vacuum influence on the material insulating performances. Thus, we have performed computations for the standard configuration ($D_p=10$ nm; $(D_c/D_p)_1=(D_c/D_p)_2=0.2$; $D_i=1.8$; $k_0=1.1$, $N_p=88$) and gas pressure between 1 bar and 1 mbar.

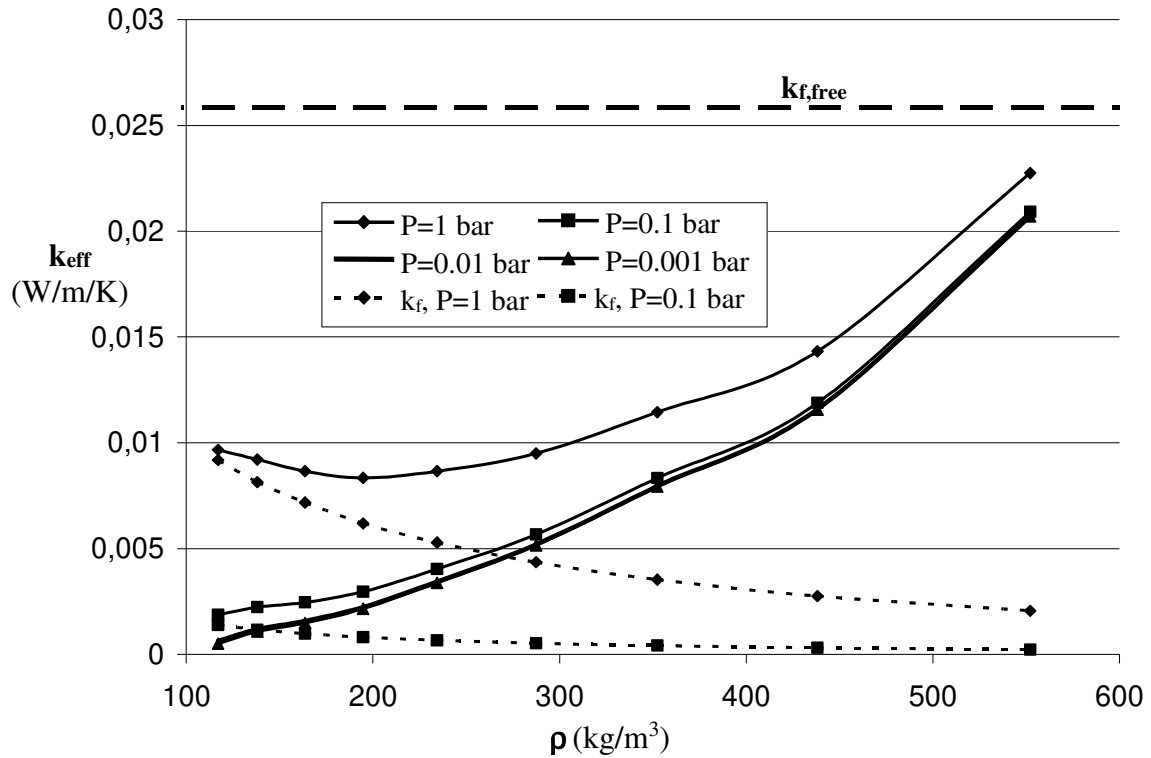


Figure 17: Evolution of the effective conductivity with the pressure of the confined gas for an agglomeration of aggregates with $D_p = 10$ nm; $D_f=1.8$; $k_0=1.1$, $N_p=88$

The graphs of Fig. 17 confirm that establishing a partial vacuum inside nano-structured silicas allows significant reduction of the effective conductivity. Actually, a partial vacuum of 0.01bar is sufficient to render the fluid phase thermal conduction almost null even for materials with low densities. Therefore, additional gas pressure reductions do not improve the insulating performances. One can also notice that, for materials with low densities and $P > 0.1$ bar, the heat propagation is almost entirely due to gas conduction. This contribution decreases with increasing density since the characteristic pore size is reduced during the compression, while, at the same time, the solid conduction is increased. As a result, one can remark the existence of optimal density guaranteeing for minimal effective conductivity at atmospheric pressure.

3.2.5 Influence of the aggregates fractal characteristics

We have varied the fractal characteristics D_f , k_0 and N_p around reference values proposed by previous studies [22, 23], i.e., $k_0 \approx 1.1$, $D_f \approx 1.8-2$ and $N_p \approx 88$. The comparison

of the obtained results assuming $(D_c/D_p)_1=(D_c/D_p)_2=0.2$ ($k_{p \rightarrow p,1} = k_{p \rightarrow p,2} \approx 0.18$ W/m/K); $D_p=10$ nm and $P=10$ mbar are illustrated on Fig. 14.

It is interesting to notice that the increase of k_{eff} with ρ appears to be dependent on the fractal characteristics (D_f , k_0 , and N_p) and essentially on the fractal dimension D_f . The differences are significant especially for the lowest densities, i.e. for non-compressed arrangements. These differences at relatively low densities can be explained by the fact that the porosities of non-compressed arrangements can be significantly different depending on the fractal dimension, while, the mean number of neighbours for a given particle is almost identical. Actually, as shown in section 2.1, aggregates with relatively high D_f have a higher compacity and lead to non-compressed arrangements with lower density. But the magnitude of heat transport due to particle-particle exchange is the same order of magnitude for the different fractal dimensions as it can be seen of Fig. 14. One can also observe that the differences between the evolutions of k_{eff} computed for different fractal dimension become quite negligible when the density becomes higher than 300 kg/m³. This can be explained by the fact that the compression process modifies the structure of the aggregates and their fractal characteristics. So, whatever the fractal characteristics of the aggregates, they all tend to the same morphology when compressed.

As a conclusion, it seems that aggregates with high fractal dimension D_f are preferable for minimizing the heat transfer through nano-structured silicas especially for relatively low densities. For relatively high densities, the fractal characteristics have only a weak influence on the insulating performances.

4 Conclusions

We have developed a parametric model for estimating the thermal behavior of nano-structured silica-based materials; that model takes into account a faithful representation of the

complex porous structure. Several conclusions on heat transfer in nano-structures silica-based materials can be drawn from the analysis of our numerical results.

At nanometric scale:

- The “nanoscopic effects” due to the very small dimensions of the silica particles remain relatively limited for silicas in commercial VIPs (according to literature $D_p \approx 10$ nm). Actually, a particle diameter of 10 nm is the limit size below which the macroscopic heat conduction law could no more be valid. For smaller particle sizes, the heat transfer predicted using Fourier law is overestimated.
- The magnitude of heat exchange between neighboring particles is mainly dictated by their contact area and varies almost linearly with it. Hence, it is essential to be able to estimate accurately this parameter.

At microscopic scale:

- The developed models clearly demonstrate that the use of nano-structured silicas permits to reach effective conductivities levels lower than that of free air ($\approx 25 \text{ mW/m/K}$) due to the very small porosity size, even at atmospheric pressure. Under partial vacuum the fluid phase conductivity is reduced even more. However, below a pressure of 10 mbar, the fluid phase conductivity can be considered null and no additional reduction can be expected.
- The insulating performances of the nano-structured silica based materials are mainly governed by the contact area of neighbouring silica particles. Moreover, the differentiation between particle-particle links inside a common aggregate or inter-aggregate links also influences significantly the effective conductivity. Actually, it seems indispensable to be able to estimate accurately the ratio $(D_c/D_p)_1$ et $(D_c/D_p)_2$ in order to obtain a satisfying predictive model.

- Our model highlights the influence of the aggregates compression on the effective conductivity. The compression leads to an increase of the mean number of contacts between particles and thus to an intensification of the heat exchange.
- The aggregates fractal characteristics (mainly the fractal dimension D_f) have an influence on the effective conductivities especially at low level of compression. High D_f tends to improve the insulating performances of the nano-structured silicas. The differences decrease with compression level and the fractal characteristics have almost no more influence for density above 300 kg/m^3 .
- Given that the “nanoscopic effects” are relatively limited for $D_p \approx 10 \text{ nm}$, the particle diameter weakly influences the heat transfer when a 10 mbar partial vacuum is applied since the fluid conductivity is almost null. On the other hand, at atmospheric pressure the particle diameter affects the insulating performances more significantly since the characteristic pore size and thus the “Knudsen effect” is directly related to this parameter.

In order to summarize the importance of the different parameters on the insulating performances of nano-structured silicas, we have established a classification of the most influent parameters in decreasing order:

1. Density
2. Partial pressure of fluid phase (air)
3. Contact area of « intra-aggregate » links
4. Contact area of « inter-aggregate » links
5. Fractal characteristics of aggregates
6. Size of silica particles

However, some future developments are envisaged in order to improve the current model:

- It seems essential to incorporate the presence of adsorbed water in the computation of the effective conductivity since nano-structured silicas constitute a hydrophilic material.
- It would also be interesting to conduct the computations using other representations of the aggregates no longer based on fractal characteristics (D_f , k_0 , N_p) but rather on the coordination number, i.e. the mean number of particle-particle contacts for each particle. Indeed, this parameter is expected to be of paramount importance
- Another next step will be to validate the present modelling results by experimental measurements.

REFERENCES

- [1] M. G. Kaganer, “Thermal Insulations in Cryogenic Engineering”, Israel Program for Scientific Translations, 1969.
- [2] Quenard D. and Sallée H., “MICRO-NANO POROUS MATERIALS FOR HIGH PERFORMANCE THERMAL INSULATION”, Proceedings of the 2nd International Symposium on Nanotechnology in Construction, Euskalduna Palace Bilbao - Spain ,13th - 16th November 2005.
- [3] Rettelbach T., Sauberlich J., Korder S. and Fricke J., “Thermal conductivity of IR-opacified silica aerogel powders between 10 K and 275 K”, J. Phys. D: Appl. Phys. Vol. 28, Issue 3, (1995), pp 581-587
- [4] R. Caps, U.Heinemann, M.Ehrmantraut, J.Fricke, 'Evacuated insulation panels filled with pyrogenic silica powders : properties and applications', High Temperatures- High pressures, 33, (2001), 151-156
- [5] R. Caps, J. Fricke, “Thermal Conductivity of Opacified Powder Filler Materials for Vacuum Insulations”, International Journal of Thermophysics, Vol. 21, n°2, (2000)
- [6] Schwab H., Heinemann U., Beck A., Ebert H.P. and Fricke J.,“ Dependence of Thermal Conductivity on Water Content in Vacuum Insulation Panels with Fumed Silica Kernels”, Journal of Building Physics, Vol. 28, No. 4, (2005), pp. 319-326

- [7] R. Coquard and D. Quenard, « Modeling of Heat Transfer in Nanoporous Silica - Influence of Moisture» Proceeding of the 8th International Vacuum Insulation Symposium 18th - 19th September 2007, in Würzburg, Germany
- [8] Rochais D., Domingues G. and Enguehard F., “Numerical simulation of thermal conduction and diffusion through nanoporous superinsulating materials”, Proceedings of the Seventeenth European Conference on Thermophysical Properties, Bratislava, 2005
- [9] S. Spagnol, “Transferts conductifs dans des aérogels de silice, du milieu nanoporeux autosimilaire aux empilements granulaires”, thèse de doctorat, Institut National des Sciences Appliquées (INSA) de Toulouse, Université de Toulouse, France, 2007
- [10] C. Kittel, « Interpretation of the thermal conductivity of glasses », *Phys. Rev.* 75, 972 1949, pp. 972-974
- [11] G. Domingues, S. Volz, K. Joulain, and J.J. Greffet, “Heat Transfer between Two Nanoparticles Through Near Field Interaction”, *PHYSICAL REVIEW LETTERS PRL* 94, 085901 (2005)
- [12] G. Domingues, D. Rochais, S. Volz, “Thermal contact resistance between two nanoparticles”, *Journal of Computational and Theoretical Nanoscience*, Volume 5, Number 2, February 2008 , pp. 153-156
- [13] S.S. Mahajan and G. Subbarayan, “Estimating thermal conductivity of amorphous silica nanoparticles and nanowires using molecular dynamics simulations”, *PHYSICAL REVIEW E*, 76, 056701 (2007)
- [14] Mazumder S. and Majumdar, A., 2001, “Monte Carlo Study of Phonon Transport in Solid Thin Films Including Dispersion and Polarization,” *ASME J. Heat Transfer*, 123, pp. 749–759.
- [15] D. Lacroix, K. Joulain, D. Terris and D. Lemonnier, « Monte Carlo transient phonon transport in silicon and germanium at nanoscales », *PHYSICAL REVIEW B* 72, 064305 (2005)
- [16] D. Lacroix, K. Joulain and D. Lemonnier, “Monte Carlo simulation of phonon confinement in silicon nanostructures: Application to the determination of the thermal conductivity of silicon nanowires” *APPLIED PHYSICS LETTERS* 89, 103104 (2006)
- [17] Randrianalisoa J. and Baillis D., “Monte Carlo Simulation of Steady-State Microscale Phonon Heat Transport Heat conduction in submicron crystalline materials ,” *ASME J. Heat Transfer*, 130, 072404, July 2008.
- [18] Randrianalisoa J. and Baillis D., “Prediction of thermal conductivity of nanostructures: Influence of phonon dispersion approximation,” *International Journal of Heat and Mass Transfer*, Vol. 52, Issues 11-12, May 2009, pp. 2516-2527.
- [19] Randrianalisoa J. and Baillis D., “Monte Carlo simulation of cross-plane thermal conductivity of nanostructured porous silicon films,” *Journal of Applied Physics*, 103, 053502 (2008)

- [20] Randrianalisoa J. and Baillis D., "Combined Analytical and Phonon-Tracking Approaches to Model Thermal Conductivity of Etched and Annealed Nanoporous Silicon", *Advanced Engineering Materials*, Vol. 11, Issue 10, October 2009, pp. 852-861
- [21] F. Enguehard, "Multi-scale Modeling of Radiation Heat Transfer through Nanoporous Superinsulating Materials", *International Journal of Thermophysics*, Vol. 28, No. 5, October 2007, pp. 1693-1717
- [22] S. Lallich, F. Enguehard, and D. Baillis, "Radiative Properties of Silica Nanoporous Matrices", *International Journal of Thermophysics*, vol.29, (2008), pp. 1395-1407
- [23] S. Lallich, F. Enguehard, and D. Baillis, "Experimental Determination and Modeling of the Radiative Properties of Silica Nanoporous Matrices", *J. Heat Transfer*, vol.131, No 8, (2009)
- [24] Mackowski, D. W., « Electrostatics analysis of radiative absorption by sphere clusters in the Rayleigh limit: application to soot particles » *Appl. Opt.* **34**, 3535 (1995).
- [25] Stephens, R. B., 1973, "Low-Temperature Specific Heat and Thermal Conductivity of Noncrystalline Solids," *Phys. Rev. B*, Vol. 8, pp. 2896-2905.
- [26] J.J. Freeman and A.C. Anderson, "Thermal conductivity of amorphous solids", *Physical Review B*, October 1986, Vol. 34, N°8, pp. 5684-5690
- [27] M.S. Love and A.C. Anderson, "Estimate of phonon thermal transport in amorphous materials above 50K", *Physical Review B*, July 1990, Vol. 42, N°3, pp. 1845-1847
- [28] K. E. Goodson, M. I. Flik, L. T. Su and D. A. Antoniadis, "Prediction and Measurement of the Thermal Conductivity of Amorphous Dielectric Layers", *Journal of Heat Transfer*, MAY 1994, Vol. 116, pp. 317-324
- [29] Kittel, C , 1986, "Introduction to Solid State Physics", Wiley, New York, Chap. 17.
- [30] Hunklinger, S., Arnold, W., 1976, "Ultrasonic Measurements in Amorphous Solids," in: *Physical Acoustics*, . P. Mason and R. N. Thurston, eds., Vol. 12, pp. 155-209.
- [31] Gilroy, K. S., and Phillips, W. A., 1981, "An Asymmetric Double-Well Potential Model for Structural Relaxation Processes in Amorphous Materials," *Philos. Mag.*, Vol. B42, pp. 735-746.
- [32] Bonnet, J. P., 1991, "On the Thermally Activated Structural Relaxation in Glasses," *J. Non-crystalline Solids*, Vol. 127, pp. 227-331.
- [33] Zaitlin, M. P., Scherr, L. M., and Anderson, A. C , 1975, "Boundary Scattering of Phonons in Noncrystalline Materials," *Phys. Rev. B*, Vol. 12, pp. 4487-4492.
- [34] M.G. Holland, "Analysis of lattice thermal conductivity", *Phys. Rev.* 132 (1963) pp. 2461–2471.

- [35] Berman, R. , “Thermal Conduction in Solids”, Oxford University Press, Oxford, United Kingdom, 1976, Chap. 9, p. 23.
- [36] Jund P. and Jullien R. ., 1999, “Molecular-dynamics calculation of the thermal conductivity of vitreous silica,” Physical Review B, vol. 59, N°21, pp. 707–711
- [37] Demirel Y. and Saxenas S.C., 1996, “Heat Transfer in rarefied gas at a gas-solid interface”, Energy, Vol. 21, No. 2, pp. 99-103

Figure Captions

Figure 1: Illustration of formation process of fumed silica – Different stages of aggregation and agglomeration

Figure 2: Illustration of the structure of nano-structured silicas at the microscopic and nanometric scales

Figure 3: Illustration of 3 representative aggregates for different values of the fractal dimension and prefactor

Figure 4: Evolution of the phonon mean free path in silica with frequency

Figure 5: Evolution of the silica conductivity with temperature, predicted by the model of Goodson et al. [27]; comparison with experimental data

Figure 6: Illustration of the Monte Carlo procedure for the resolution of Boltzmann Equation for two nano-particles in contact

Figure 7: Flow-chart of the Monte Carlo procedure used for the resolution of Boltzmann Equation in the nano-structure

Figure 8: Principle of the computation of the effective thermal conductivity for the arrangement of aggregates of nano-particles using FVM

Figure 9: 2-D Illustration of the thermal balance during the Finite Volume computation

Figure 10: Illustration of a parallelepipedic volume representative of an arrangement of fractal aggregates

Figure 11: Evolution of the pore characteristic size with the solid fraction in arrangement of aggregates of different fractal characteristics

Figure 12: Evolution of the particle-particle conductivity with the particle diameter for different contact area D_c/D_p

Figure 13: Evolution of the $k_{p \rightarrow p}$ with the ratio D_c/D_p computed using MC simulations for the resolution of Boltzmann Equation or using the Macroscopic Fourier laws

Figure 14: Evolution of the effective conductivity with density for arrangements of aggregates with different fractal characteristics and assuming $D_c/D_p=0.2$ ($k_{p \rightarrow p,1} = k_{p \rightarrow p,2} \approx 0.18$ W/m/K)

Figure 15: Evolution of the effective conductivity with density as a function of the particle diameter for an arrangement of aggregates with $D_f=1.8$; $k_0=1.1$, $N_p=88$

Figure 16: Influence of the contact areas on the effective conductivity evolution for an arrangement of aggregates with $D_f=1.8$; $k_0=1.1$, $N_p=88$ and $P=10$ mbar

Figure 17: Evolution of the effective conductivity with confined gas pressure for an agglomeration of aggregates with $D_p = 10$ nm ; $D_f=1.8$; $k_0=1.1$, $N_p=88$